

Combining Multi-Wavelength AERONET SSA Retrievals with a MIE Model to Quantify the Size of Absorbing Aerosols and the In-Situ Lifetime of Sulfate

Xinying Wang¹, Jason Blake Cohen², and Shuo Wang³

¹Sun Yat-sen University

²School of Environment Science and Spatial Informatics, China University of Mining and Technology

³Chengdu University of Information Technology

November 24, 2022

Abstract

Energy, transport, urbanization and burning are responsible for changes in atmospheric BC. This work uses direct solar atmospheric column measurements of single scatter albedo [SSA] retrieved at multiple wavelengths from AERONET at 68 Asian sites over 17 years. A MIE model is solved across the wavelengths using a core-shell mixing approximation to invert the probabilistic BC, shell size, and UV SSA. Orthogonal patterns are obtained for urban, biomass burning [BB], and long-range transport [LRT] conditions, which are used to analyze and attribute source types of BC across the region. Large urban areas (thought to be dominated by urban BC) are observations during targeted times (shorter than seasonally) to yield significant contributions from non-urban BC. BB and LRT are observed to dominate Beijing and Hong Kong 2 months a year. LRT is observed during the clean Asian Monsoon season in both Nepal and Hong Kong, with sources identified from thousands of kilometers away. Computing the shift in shell size required to constrain the results approximates secondary aerosol growth in-situ, and subsequently aerosol lifetime, which is found to range from 11 days to a month, implying both a significant amount of BC above the boundary layer, and that BC generally has a longer lifetime than PM_{2.5}. These findings are outside of the range of most modeling studies focusing on PM_{2.5}, but are consistent with independent measurements from SP2 and modeling studies of BC that use core-shell mixing together with high BC emissions.

1
2 **Combining Multi-Wavelength AERONET SSA Retrievals with a MIE Model**
3 **to Quantify the Size of Absorbing Aerosols and the In-Situ Lifetime of Sulfate**

4 **Xinying Wang¹, Jason Blake Cohen^{2*}, Shuo Wang³**

5 ¹School of Atmospheric Sciences, Sun Yat-Sen University, Guangzhou, China.

6 ²School of Environment and Spatial Informatics, China University of Mining and Technology,
7 Xuzhou, China.

8 ³School of Electronic Engineering, Chengdu University of Information Technology, Chengdu,
9 China.

10 Corresponding author: Jason Blake Cohen (jasonbc@alum.mit.edu)

11 **Key Points:**

- 12 • Urban sites throughout Asia are impacted not only by local sources but also biomass
13 burning and sources conveyed long-range transport.
- 14 • Quantifies the age and attributes the sources as a function of time based on multiple
15 wavelength analysis.
- 16 • Uncertainty analysis indicates that the number of very small particles and total absorption
17 are underestimated by surface measurements.

18 **Abstract**

19 Energy, transport, urbanization and burning are responsible for changes in atmospheric BC. This
20 work uses direct solar atmospheric column measurements of single scatter albedo [SSA]
21 retrieved at multiple wavelengths from AERONET at 68 Asian sites over 17 years. A MIE model
22 is solved across the wavelengths using a core-shell mixing approximation to invert the
23 probabilistic BC, shell size, and UV SSA. Orthogonal patterns are obtained for urban, biomass
24 burning [BB], and long-range transport [LRT] conditions, which are used to analyze and
25 attribute source types of BC across the region. Large urban areas (thought to be dominated by
26 urban BC) are observations during targeted times (shorter than seasonally) to yield significant
27 contributions from non-urban BC. BB and LRT are observed to dominate Beijing and Hong
28 Kong 2 months a year. LRT is observed during the clean Asian Monsoon season in both Nepal
29 and Hong Kong, with sources identified from thousands of kilometers away. Computing the shift
30 in shell size required to constrain the results approximates secondary aerosol growth in-situ, and
31 subsequently aerosol lifetime, which is found to range from 11 days to a month, implying both a
32 significant amount of BC above the boundary layer, and that BC generally has a longer lifetime
33 than PM_{2.5}. These findings are outside of the range of most modeling studies focusing on
34 PM_{2.5}, but are consistent with independent measurements from SP2 and modeling studies of BC
35 that use core-shell mixing together with high BC emissions.

36 **Plain Language Summary**

37 Energy, transport, urbanization and burning are responsible for significant changes in
38 atmospheric Black Carbon aerosol [BC]. This study analyzes atmospheric column measurements

39 using different parts of the solar spectrum with a physical model, to describe the solution set of
40 BC and coating sizes in the atmosphere. This information is then used to make different aerosol
41 types, including urban, biomass burning, and aerosols which have been in the atmosphere for a
42 very long time. These type profiles are applied throughout Asia to analyze the sources of BC.
43 While many sites are as expected, most large urban areas are observed to have both biomass
44 burning and long-range transport types found when looking over short time periods which occur
45 annually. Next, even during heavy Monsoon rains, urban areas are found to have significant
46 amounts of long-range transported BC. The lifetime of the BC is also obtained from the growth
47 in the shell size, demonstrating that BC stays in the atmosphere longer than current studies
48 focusing on PM_{2.5} can observe. Focusing models more specifically on BC, formulating different
49 controls during different periods of the year, and better studies of BC emissions could all yield
50 improved understanding of BC and its effects.

51 **1 Introduction**

52 Black carbon (BC), organic carbon (OC) and dust (or Absorbing Aerosols - AA) can
53 strongly interact with solar radiation, leading to impacts on the atmospheric radiation budget,
54 climate, water cycle, and more (Jacobson, 2001; Menon et al., 2002; Wu et al., 2008). Black
55 Carbon can absorb solar radiation strongly in the visible and infrared. Small changes in BC
56 loadings can cause a significant change in the local solar radiation absorption and hence altering
57 the regional and global climate (Ramanathan et al., 2001a, 2001b). This interaction critically
58 relies on the particle size distribution, chemical composition and mixing state in-situ (Jacobson,
59 2001). The two most significant difficulties in estimation of the climate effects of black carbon
60 are the variable physical-chemical properties of BC-containing particles (Miyakawa et al., 2017)
61 and the heterogeneous distribution (Bollasina et al., 2013; Shen Z et al., 2020; Cooke et al.,
62 2002; Lu et al., 2011). While BC itself is water-insoluble once it has been in the atmosphere for a
63 long enough time, it will become coated (Zhang et al., 2016; Cohen and Wang, 2014) in turn
64 becoming hygroscopic (McMeeking et al., 2011) and therefore having the potential to impact
65 climate via wet and ice clouds (Penner et al., 1992; Penner et al., 2001; Kuwata et al., 2007). Due
66 to its long lifetime in the atmosphere, BC has also been known to travel very long distances,
67 impacting regions thousands of km away from the source region, and undergoing in-situ
68 processing such that its absorbance and impact on clouds may both be enhanced, further
69 impacting the radiative balance over large scales (Liu et al., 2011; Zhang et al., 2015; Prasad et
70 al., 2018; Guha et al., 2015; Wang et al., 2009). Taking all of these factors into consideration, the
71 current range of radiative forcing estimates of BC (at TOA) range from +0.13 to +1.4 W/m²
72 (Haywood and Shine, 1995; Haywood et al., 1997; Haywood and Ramaswamy, 1998; Myhre et
73 al., 1998; Penner et al., 1998; Cooke et al., 1999; Jacobson, 2000; Wang, 2004; Wang et al.,
74 2014; Jacobson et al., 2001; Bond et al., 2013; Cohen et al., 2011).

75 Attempts have been made to elucidate particle size, mixing state, emissions, and aging
76 over highly polluted regions in Asia using different models and methods (Salam et al., 2012;
77 Quinn et al., 2004; Kompalli et al., 2021; Han et al., 2013; Streets et al., 2003; Kühn et al., 2014;
78 Xu et al., 2015; Song et al., 1999). However, at the present time there are few if any studies that
79 have comprehensively focused on the long-term properties of the particle size and source (i.e.
80 distance to a biomass burning or urban source) and aging (i.e. how long the aerosol has
81 undergone processing and deposition in-situ). Studies which have analyzed aerosols using
82 remote sensing have tended to focus on the visible and IR radiative bands, with measurements
83 from the UV band scarcely used (Corrigan et al., 2006). In specific, many present remote sensing

84 based studies merely focus on a fine mode and coarse mode (Eck et al., 2010; Koulouri et al.,
85 2008; Zhang et al., 2017; Kleidman et al., 2005). Attempts have also been made via field
86 observations. Schwarz et al (2008) used an airborne single-particle soot photometer to quantify
87 BC aerosol microphysical state in fresh urban and BB emissions. These differences contribute to
88 significant impacts on the BC size distribution and concentration, when observed using
89 measurements based on particulate absorption (Sato et al., 2003). However, results such as these
90 from both remote sensing and field studies are not considered in most chemical transport and
91 aerosol models today, which tend to not assume a Core-Shell approximation which in turn tends
92 to underestimate the overall absorption profile, requiring scaling to match optical properties such
93 as SSA, AAOD and size information (Myhre et al, 1998; Cooke et al.,1999; Jacobson et al.,
94 2000; Wang et al., 2009; Cohen et al 2011). Consequently, these models tend to underestimate
95 ultra-long-range transport and non-local polluted conditions, frequently induced by vertical
96 transport and aging associated with underestimated absorption (Wang et al., 2020). It has been
97 demonstrated that a Core-Shell model fits best with aerosol properties in heavily polluted region
98 such as East, Southeast and South Asia where sulfate or nitrate can coat on BC in a short time
99 after it has been emitted, consistent with the fact that in these parts of the world biomass burning
100 sources and urbanization are located in close proximity to each other (Cohen and Wang, 2014;
101 Peng et al., 2016; Zhang et al., 2016; Cohen et al., 2017).

102 To achieve a better understanding of AA and its impact on the atmosphere, this work
103 incorporates multi-spectral atmospheric column high frequency measurements and inversion
104 products from AERONET including AOD and SSA, as well as mixing state and size
105 measurements from ground station, in connection with a inverse constrained variance
106 maximization approach to reveal size and absorption properties of aerosols in Asia. A specific
107 focus is made on the added value of using measurements in the UV bands which provides deeper
108 support for and quantitative insight into the loadings and sizes of smaller particles, allowing for
109 better characterization of both aging as well as fresher particles. The inversely constrained
110 particulate core and shell sizes based on the SSA values from the Mie model and constrained
111 by AERONET, allow for a new categorization of aerosols based on whether they are
112 emitted locally in Urban areas [Urban], have undergone Long-Range Transport [LRT], or are
113 emitted locally by Biomass Burning [BB]. The approach also allows a statistical solution space
114 to indicate the range of mixtures of these source types which would also be capable of being
115 physically realistic, taking into the specific particle size (both core and shell) distribution. This
116 allows the use of typical and well classified sites to be used to improve understanding of
117 different sources and their contributions to the atmospheric loading, as well as impacts on
118 radiative forcing and subsequently on climate change. Since these are based on column
119 measurements of the entire atmosphere, they provide important support to further promote
120 improvement of models, in terms of capturing the total atmospheric loading, attribution of
121 extreme or abnormal events, and impacts of high-frequency changes on the overall performance of
122 models, all of which are cited as important weaknesses of current aerosol modeling systems.
123 Some specific scientific points of interest discovered include quantification of significant events
124 in which mixing occurs between an expected and an unexpected source, detection of
125 missing/previously unidentified sources, details about changes in the optical and size properties
126 of aerosols which are otherwise obscured when only looking at a PM_{2.5} or Fine Mode type of
127 aerosol constraint, and quantifying of different aging rates occurring between BB and Urban
128 cases. It is finally hoped that ongoing calculations incorporating the quantitative approach
129 explicitly employed here will allow for further expansion and insights to be gained and for more

130 multi-wavelength measurement platforms of aerosol absorption to be further incorporated in the
 131 future, allowing for further understanding, advances in attribution, and improvement of models
 132 and impacts on people, health, and the climate system.

133 **2 Data and Methods**

134 2.1 AERONET Data

135 This work uses Aerosol Optical Depth (AOD) and Single Scattering Albedo (SSA) from
 136 March 1997 to May 2017 using ground-based Aerosol Robotic Network (AERONET)
 137 observations. AERONET uses CET318-TS9 instruments to provide information about the
 138 spectral sun irradiance and sky radiances at multi-bands including at wavelengths of 340 and 380
 139 (AOD only), and 440, 670, 870 and 1020nm (both AOD and SSA)
 140 (https://aeronet.gsfc.nasa.gov/new_web/data_description_AOD_V2.html). This work uses level
 141 2.0 cloud screened and quality assured data (Holben et al., 2006), focusing on the time variations
 142 and loading/magnitude of the daily mean measurements over the entirety of the time series which
 143 have three or more individual measurements available within the time of one calendar day. To
 144 avoid the case where there is a weak signal and ensure sites have sufficient data to capture the
 145 feature of each site, all AERONET sites were filtered previous to classification, only retaining
 146 sites that have 100 or more days of data in addition to at least one of three conditions: high mean
 147 AOD, high extreme event AOD, or highly variable AOD. If a site has more than 300 days of
 148 total data (Wang et al., 2021; Dubovik and King et al., 2000; Dubovik et al., 2002), then the site
 149 is also used, even if it does not meet one of the three conditions. After filtering 68 sites remain
 150 for further analysis throughout East Asia, Southeast Asia, South Asia, Eastern Russia, and
 151 Australia. Furthermore, other than sites located in Western India and Western China, the
 152 remainder of the sites in this analysis do not generally have a significant dust loading, and
 153 therefore the major source of absorption is assumed to be black carbon (BC), allowing this work
 154 to assume a direct relationship between BC and SSA (Cohen and Wang, 2014).

155 2.2 Mie Model

156 A Mie model is used to connect the radiative measurements and observations from
 157 AERONET with approximations of the various optical, mixing state, and implied chemical
 158 properties of the aerosols. Mie Theory solves the aerosol optical properties based on a given size
 159 and optical distribution of particles, following Bohren and Huffman (1983). It assumed the time
 160 variation of the field is $\exp^{-i\omega t}$, leading exclusively to positive imaginary parts of the refractive
 161 index corresponding to absorbing media. Although externally, internally and core-shell mixtures
 162 are frequently used to characterize particle morphologies and chemical compositions (Cheng et al.,
 163 2008; Lin et al., 2013; Tao et al., 2019; Zhang et al., 2017), this work assumes that all the
 164 particles have a Core-Shell structure, which has been demonstrated to be reasonable in urban
 165 areas in Asia based on both modeling and measurement studies (Cohen et al., 2011; Cohen and
 166 Wang, 2014; Zamora et al., 2019), as well as being compatible with the AERONET inversion
 167 technique (Dubovik, 2002).

168 Using particle size and refractive indices, this work computes the extinction coefficient
 169 (Q_{ext}), scattering coefficient (Q_{sca}) and absorbing coefficient (Q_{abs}). The resulting single-
 170 scattering albedo (SSA) is calculated based on the equation (1) (Hansen et al., 2009).

$$SSA = \frac{SCATTERING}{EXTINCTION} = \frac{Q_{sca}}{Q_{ext}} \#(1)$$

171 Since AERONET does not report the SSA in the UV band, this work computes the SSA field
 172 using the MIE model at 340nm using a core-shell approximation where the aerosols contain a
 173 pure BC core with a scattering (i.e. Sulfate or Nitrate) coating, where the core refractive index is
 174 $2.0+1.0i$ (Schuster et al., 2005) and the shell refractive index is $1.52-5*10^{-4}i$ (B Aouierats et al.,
 175 2010). This is physically consistent with the facts that many primary aerosols in these regions are
 176 organic and that they age rapidly as a function of their time in-situ (Cohen and Wang, 2014; May
 177 et al., 2015; Song et al., 1999). The model computes particle sizes of the core in steps of $0.01\mu\text{m}$
 178 from $0.05\mu\text{m}$ to $0.50\mu\text{m}$, and the shell in steps of $0.01\mu\text{m}$ from $0.01\mu\text{m}$ to $0.80\mu\text{m}$.

179 2.3 Copernicus Atmosphere Monitoring Service (CAMS) SO₂ data

180 CAMS global reanalysis product provides monthly average SO₂ at $0.75^\circ \times 0.75^\circ$ resolution
 181 ([https://ads.atmosphere.copernicus.eu/cdsapp#!/dataset/cams-global-reanalysis-eac4-](https://ads.atmosphere.copernicus.eu/cdsapp#!/dataset/cams-global-reanalysis-eac4-monthly?tab=overview)
 182 [monthly?tab=overview](https://ads.atmosphere.copernicus.eu/cdsapp#!/dataset/cams-global-reanalysis-eac4-monthly?tab=overview)). This study uses data from 2019 data over 7 vertical levels from the
 183 surface to 700hPa. Additional measurements of SO₂ at the surface are obtained over China from
 184 the Ministry of Ecology and Environment of the People's Republic of China.

185 2.4 Single Particle Soot Photometer (SP2) Measurement

186 SP2 measures individual aerosol particles. These measurements are capable of determining
 187 the optical size and characteristics by scattering and absorption using 1040nm radiation, as well
 188 as induced laser incandescence of pure carbon-containing cores. In the real atmosphere at these
 189 wavelengths, the major source of absorption corresponds to BC (Bond, T.C., et al., 2013; Bond
 190 and Bergstrom, 2006; Bond, 2001; Penner, 1994), which can then be converted into a core
 191 diameter (D_c) using a mass equivalent diameter ($\rho=1.8\text{g}/\text{cm}^3$ for atmospheric BC) and assuming
 192 that BC is spherical (Martins et al., 1998; Smith and Grainger, 2014; Jacobson and M.Z., 2000,
 193 2001). The optical diameter of the non-BC portions of the particle (D_p) is calculated using Mie
 194 theory, and presented as (D_p/D_c).

195 This study used SP2 data measured by the Institute of Atmospheric Physics Beijing
 196 ($39.58'28''\text{N}$, $116.22'16''\text{E}$) observed from 2016.11.10 to 2017.09.15. This specific location is
 197 located very close to an AERONET station in Beijing (39.977N , 116.381E) which has
 198 measurements in 2001 (March to May), 2015 (September to December) and 2016 (January to
 199 July). There is an overlap between these two datasets from 2016.11.10 to 2017.01.12, which
 200 hereafter is used for the comparison between D_p/D_c inverted from AERONET and measured by
 201 SP2.

202 2.5 In-situ lifetime calculation

203 Considering that a minimum concentration of sulfuric (or nitric) acid is required before BC
 204 can age, the lifetime of SO₂ provides an excellent proxy to approximate the time in-situ. This can
 205 be quantified following Equation 2 where M is the SO₂ concentration, and k is the rate constant.

$$\frac{D[M]}{Dt} = -k[M] \quad (2)$$

206 The solution of Equation 2, after rearrangement of the terms is given in Equation 3 where k
 207 equals to t/τ , t is the in-situ time the particle spent in the atmosphere, τ is the e-folding time of
 208 SO₂ in-situ, $M(\text{env.})$ is the mean environmental concentration of SO₂ encountered by the particle,
 209 and $M(\text{growth})$ is calculated based on the [BB] Profile (more details in 4.1), based on the average
 210 atmospheric concentration of sulfate in the region studied being about $2.9\mu\text{g}/\text{m}^3$.

$$t = \frac{-\ln \frac{M(\text{growth})}{M(\text{env.})}}{\tau} \#(3)$$

211 In the background case, the assumed lifetime of SO₂ is 1.56 days (Pham et al., 1995; Chuang
 212 et al., 1997; Chin et al., 1996; Croft et al., 2014; Restad et al., 1998). In the urban case, the
 213 lifetime is expected to be shorter, since the loading of OH is higher and conversion to H₂SO₄ gas
 214 and subsequent gas to particle conversion is faster (Cohen et al., 2011; Liu et al., 2018; Saiz-
 215 Lopez et al., 2017; Saxena et al., 1987). This work recalculates the e-folding time assuming that
 216 Beijing is a representative site for urban chemistry. Based on the Beijing high time profile
 217 obtained by extracting the size value in the peak period (25 days in total) and the ground
 218 measurements of SO₂ from the China EPA Beijing station, the urban lifetime is computed to be
 219 approximately 0.98 days.

220 2.6 Statistics and analytics used in this work

221 Considering that many sites in the region are undergoing rapid change and might have
 222 different characteristics during different time periods, a method is derived to look at extremely
 223 polluted days separately from the non-polluted days. This selection of heavily polluted days is
 224 made by defining the peaks of the data greater than the mean plus one standard deviation,
 225 removing these, and re-iterating 3 times. The net aggregation of those days is herein considered
 226 heavily polluted.

227 3 Analyses of selected regions

228 3.1 Time series of selected cases

229 The temporal characteristics of daily average AERONET AOD (340nm) over different times
 230 are given in Figure 1, with non-polluted values shown in green, while those considered heavily
 231 polluted are uniquely represented as blue, black, and red respectively based on being filtered
 232 during the first, second, and third passes respectively. Common features observed include
 233 relatively regular signals of an annual peak and trough with a roughly similar start time, end time
 234 and duration. Some sites occasionally have large values and otherwise are relatively low or
 235 moderate in terms of AOD, but without any clear pattern (these patterns do not have any clear
 236 start or end time, duration, magnitude, or extremum), leading to the changes being associated
 237 with some process that locally varies significantly from time to time, consistent with long-range
 238 transport based events. In these cases, the average AOD during the non-peak times tends to be
 239 not high. In addition to the above situations, sometimes the distribution of AOD is completely
 240 irregular, with no obvious pattern during either the cleaner periods or the peak periods, and no
 241 obvious pattern in terms of high or low magnitude. In this case, the source region is more likely
 242 to be urban in nature, because urban emissions exist year-round without a large amount of
 243 variation, although small changes due to the day of the week, the season of the year, and local
 244 meteorology combine to provide temporal variability.

245 Chiangmai is the biggest city in northern Thailand and is the only location in Northern
 246 Thailand, Myanmar, or Laos with an industrial presence (population of 127,000). However,
 247 based on previous work (Lin and Cohen et al., 2020; Wang and Cohen et al., 2020; Cohen et al.,
 248 2017), this region generally has industrial and urban signals of emissions which are very small,
 249 instead having a signal dominated by biomass burning. Based on Figure 1a, the time series of

250 Chiangmai has a very unique feature with most of the year being relatively clean, and a short but
251 intense time during which it is extremely polluted. The peak always occurs during roughly the
252 same time (From February through 19 April) every year over the entirety of the 10 years of
253 measurements, and furthermore a peak never occurs outside of this time. Given this and the
254 previous works identified above, Chiangmai is considered the most representative region with
255 respect to biomass burning.

256 Taihu is a large lake located partially in Wuxi (7 million people) and partially in Suzhou (11
257 million people), cities which have the second and third highest per capita PPP in China. The lake
258 is located in the middle of the Shanghai, Nanjing, Hangzhou conurbation. For this reason, the
259 region has a huge amount of individual vehicles, factories, manufacturing and other economic
260 activity, yet is not adjacent to any specific road or factory. As such, it is quite representative of a
261 region in which the major source of pollution is urban, as has been shown by previous works
262 (Huang et al., 2021; An et al., 2021; Logan et al., 2013; Chen et al., 2020). As shown in Fig.
263 1(b), a time series of the AOD tends to be high on average, and contains a large amount of
264 variability that appears both random and not intensely concentrated during any specific periods
265 of time.

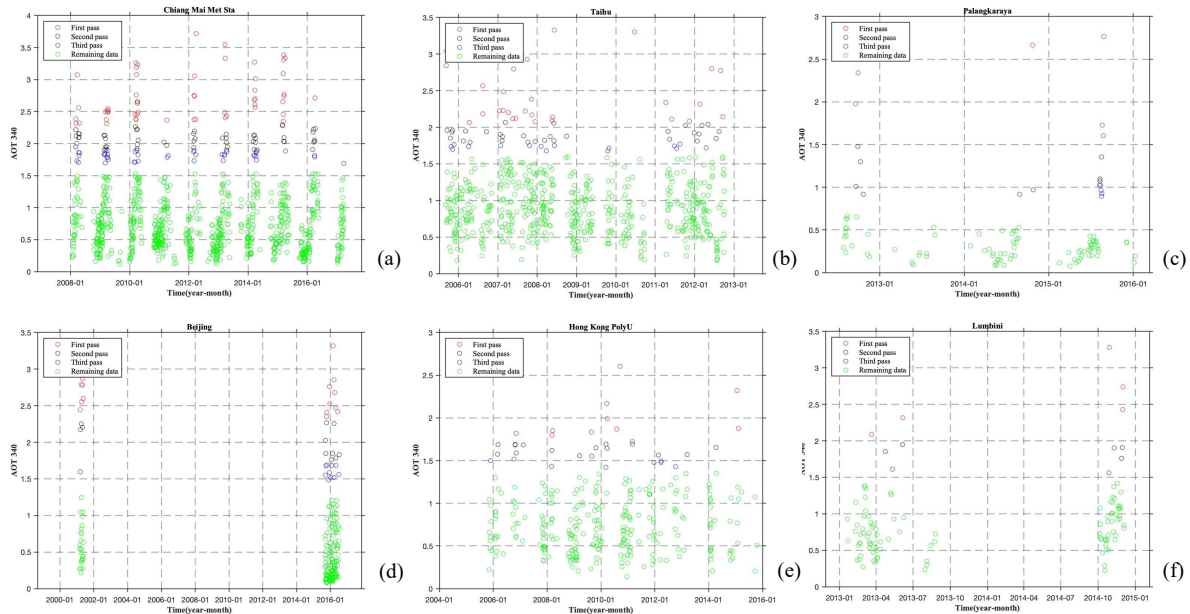
266 Palangkaraya is a small city located in southwestern Borneo, which is surrounded by forests
267 and peatlands. The city itself is not a major source of emissions, and while the surrounding land
268 had been frequently burned in the past, today it consists of plantations without any more
269 burning. The data available at this site ranges from 2012 through 2016, during which the
270 location region was already transformed into plantation (nearly no local sources), but which was
271 surrounded by generally high amounts of biomass burning hundreds to thousands of kilometers
272 away coming from elsewhere in the Maritime Continent in 2012 and 2015, as demonstrated by
273 the time series data itself, and previous studies (Deng et al., 2020; Cohen, 2014). The relatively
274 low mean and high standard deviation of AOD show a consistent pattern whereby the region is
275 impacted by long-range transport of biomass burning from other regions. Consistently there is
276 observed to be a variable start and end time changing year to year, starting as early as early
277 august and ending as late as early November. Otherwise, this region tends to have very low
278 levels of BC and generally is clean. This combination of conditions leads to it being an excellent
279 candidate to represent long-range transport.

280 Beijing as a typical megacity, with a population more than 18 million, and considerable
281 sources from high tech, industry, and government. Based on the total available three year's data
282 in 2001, 2015 and 2016 the features in general appear to be like Taihu, consistent with the
283 understanding that Beijing is also urban. The value of AOD during the highest period is about
284 3.2, while most of the second pass and third pass data fall in the range of 1.5~3, with the concept
285 that the temporal occurrence of peak events is random but tending to be of similar magnitude. In
286 addition, there is a considerable amount of the total data (37%) which behaves like long range
287 transport. This tends to occur during spring, but only occurring in specific years (Han et al., 2015;
288 Wang et al., 2015; Wang et al., 2004). This is consistent with the fact that transport from western
289 china (Shanxi, Shaanxi, Ningxia, etc.) and its large amount of energy and downstream energy
290 emissions sources, or northeastern china (and its heavy biomass burning and industrial
291 emissions) does occur at times when spillover occurs over the mountains surrounding the edges
292 of Hebei and Beijing (Li et al., 2022; Qin et al., 2022; Wang et al., 2020).

293 The temporal characteristics of AOD in the megacity of Hong Kong form another very
294 interesting case, as observed in Figure 1(e). The value tends to have a relatively high mean with
295 most measurements between 1.0 and 1.5, and seemingly occurring randomly throughout most of

296 the year. This result is consistent with its large industrial, transportation, and shipping sectors,
 297 and located in the middle of the highly populated and heavily industrialized Pearl River Delta
 298 region. However, there also is a recurring increase in the overall AOD (between 1.5 and 2.6) that
 299 occurs in October. These results are unexpected in Hong Kong when compared with many local
 300 studies (Tan et al., 2016; Fang et al., 2018; Xu et al., 2022), however they are consistent with
 301 recent studies which have focused on the changes in the Monsoon (Yang et al., 2006; Yao et al.,
 302 2008; Lau et al., 1997) and biomass burning increases throughout Northern Southeast Asia (Lin
 303 et al. 2020; Wang et al., 2021). A major difference is that these studies which have observed
 304 these changes are whole-atmospheric studies, not specifically related to measurements at the
 305 surface.

306 Lumbini in South Asia is a rapidly developing urban area in Nepal. The signal corresponds
 307 strongly with known urbanization, a high population density, and many small and randomized
 308 sources including rubbish and trash burning, small brick and cement kilns, and a growing
 309 proliferation of combustion-based transport options. The strength of the red signal varies in
 310 intensity and magnitude from an observed relative maximum in the middle and end of 2014 as
 311 development rapidly accelerated (Rupakheti et al., 2020).



312
 313 **Figure 1.** Time series of AOD at 340nm of different sites. (a) Chiang Mai Met Sta; (b) Taihu; (c)
 314 Palangkaraya; (d) Beijing; (e) Hong Kong PolyU; (f) Lumbini

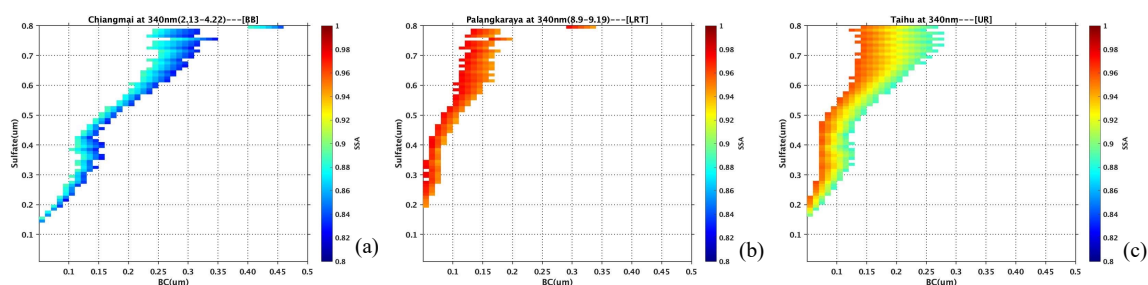
315 3.2 Typical Features of Well-Defined Source Regions

316 To calculate the typical characteristics of biomass burning, the distribution of solutions of
 317 size pairs of core and shell radius corresponding to the intersection across all different
 318 wavebands of the measured SSA in Chiangmai during the high season will subsequently be used,
 319 hereafter called [BB], see Fig.2a. Since the burning in Chiangmai is local, the profile may be
 320 used to represent other regions which also have a significant local biomass burning source. If a
 321 region has a good match with the biomass profile, it implies that the local aerosol profile is
 322 influenced by local biomass burning. When a region has a good match with the biomass profile
 323 after being shifted upwards, it is consistent with a region that is impacted by biomass burning

324 which has undergone growth in-situ while undergoing transport between its source and where it
 325 was ultimately measured. In this case, an approximation of the age of the biomass burning can be
 326 obtained indirectly by considering how much upward shift is required to make the best fit, where
 327 the shift quantifies the amount of shell growth while in-situ.

328 Similarly, the distribution from Palangkaraya is used to compute the conditions under which
 329 long-range transport occurs, subsequently called [LRT] (Wang et al., 2021), see Fig.2b. The
 330 AOD pattern of Palangkaraya shows a combination of relatively low mean and a high standard
 331 deviation of AOD, which starts and ends around the same time every year. Local measurements
 332 of CO from the long-term WMO station in the same city also has a similar signal (Aouizerats et
 333 al., 2014). Basically, the local environment is nearly pollution free, except for when biomass
 334 burning occurs on Sumatra, Borneo, and other islands in the region, which then transport to the
 335 site. For these reasons, measurements at this site are an excellent candidate to represent sites
 336 typically impacted by long-range transport.

337 Finally, the distribution of solutions of size pairs of core and shell radius corresponding to the
 338 measured SSA in Taihu referred to as [UR], see Fig.2c. Since Taihu is near the center of the
 339 world's largest conurbation, yet located in the middle of a lake, highways and other immediate
 340 point sources are reduced, making the profile highly representative of a generalized urban area.



341
 342 **Figure 2.** BC core and Sulfate shell size distributions, with corresponding SSA (color) at the
 343 three well-defined source sites: Chiangmai [BB], Palangkaraya [LRT], and Taihu [UR].

344 3.3 Quantifying New Spatial and Temporal Relationships in BC Properties Induced by 345 Various Natural and Anthropogenic Forcings

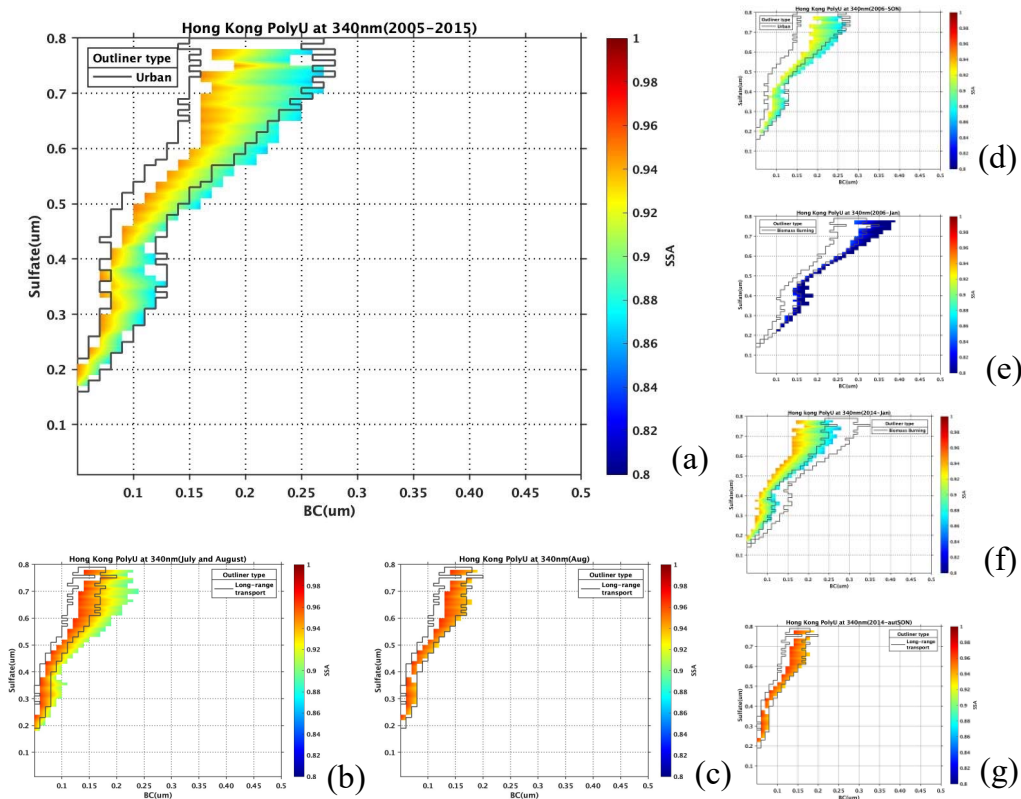
346 The climatologically constrained SSA distribution in the 126 million population Greater Bay
 347 Conurbation (hereby defined based on measurements from the Hong Kong PolyU site) is given
 348 in Fig.3a. The climatological core and shell size distributions show mostly urban characteristics,
 349 as expected from the high population density, large and growing economic footprint in this
 350 region. However, the geographical location of Hong Kong places it in a region influenced by the
 351 Asian monsoon, in a dense urban area surrounded by significant agriculture, and upwind from
 352 the rapidly developing and transforming nations in ASEAN.

353 As expected, the overall climatology of aerosol properties in Hong Kong, based on the
 354 magnitude of the SSA (i.e., color) and size distribution of both the core and shell (i.e., shape of
 355 the SSA distribution) derived over this station is mostly dominated by [Urban], with very small
 356 amounts of [LRT] and [BB] (Fig 3a). However, both inter-annual and intra-annual variability are
 357 observed to be very important in this region.

358 A first case is observed in Fig 3b-c. Monsoon theory indicates that there is a strong Southeast
 359 wind occurring in July and August, leading to flow from the clean South China Sea to the
 360 Chinese Mainland, with Hong Kong being one of the first points of contact (Yang et al., 2014;

361 Lawrence and Lelieveld, 2010; Webster and Yang, 1992; Zhu et al., 2012). It has generally
 362 implied that during this time, the air should be extremely clean. And when analysis is done using
 363 all days from July and August as given in Fig 3b, the local signal is observed along with an LRT
 364 signal. However, a look at only the August data reveals a pure LRT signal (Fig.3c). Since the
 365 winds are not changing during this period of time, therefore the results are consistent with a
 366 significant change in the aerosol loading on the southern edge of the South China Sea. This is
 367 consistent with known massive fire events which occur starting in August on a nearly annual
 368 basis (Deng et al., 2021; Cohen, 2014; Cohen et al., 2017; Wang et al., 2020; Li et al., 2020;
 369 Chen et al., 2017). This data offers a first independent characterization of significant long range
 370 transport of biomass burning absorbing aerosol over 2000km from Borneo to Hong Kong.

371 Furthermore, it can be seen in Figs 3d-g that in 2006 the [Urban] source occupies the vast
 372 majority of the September/October/November signal, with a very small amount of BB mixed in,
 373 while the September/October/November signal in 2014 is found to mostly consist of LRT with
 374 only a small amount of Urban. Similarly, the January signals in 2014 and 2006 are also vastly
 375 different from each other, with 2014 being mostly Urban in nature, and 2006 having an
 376 extremely strong BB signal. All of these results are consistent with the fact that 2006 was a
 377 strong El-Nino and 2014 was a mixture of a budding La-Nina occurring at the same time as a
 378 negative IOD (Logan et al., 2008; Deng et al., 2021; Cohen, 2014; van der Werf et al., 2008;
 379 Rinsland et al., 2008; Chi et al., 2019; Xie and Fang, 2019).



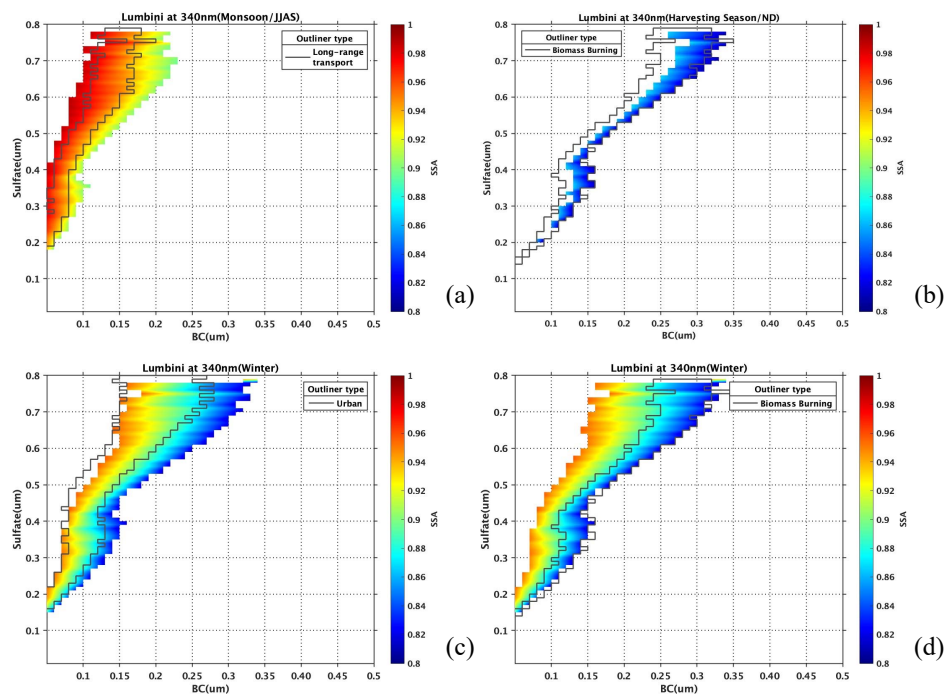
380
 381 **Figure 3.** Constrained distribution of SSA from model result of Hong Kong PloyU during
 382 different special time periods with urban, Biomass Burning and Long-range transport profile.

383 Lumbini is located in Nepal and represents the densely populated Southern Slopes of the
384 Himalayas, a region impacted by biomass burning, the Monsoon, and very large variance in
385 aerosol loadings from ultra clean to some of the most polluted conditions on the planet. Fig 4
386 shows the constrained SSA distribution during three seasons where there are vastly different
387 conditions observed.

388 First during the monsoon season (JJAS) the majority of the sources are influenced by long
389 range transport, consistent with the squeezing of air from the Continent into the foothills of the
390 Himalayas (Dumka et al., 2015; Rupakheti et al., 2017; Rupakheti et al., 2020; Chen et al.,
391 2020). During this time, a mixture of long-range transport and urban aerosols are observed, with
392 the solution covering a very wide range of particle radii from 210nm up to 1030nm. This result is
393 consistent with the site being impacted by air masses both of a local origin as well as those
394 having been transported very far away from regions with a very high loading. These results are
395 consistent with the rapid onset in terms of wind speeds, and consistent direction from south to
396 north. Localized fires, coupled with urban areas in Eastern India and Bangladesh are all upwind
397 from Lumbini during this time. It is important to note that while heavy rain removes aerosols
398 during this time of the year, that it also does not rain 24 hours a day 7 days a week over the entire
399 domain, and therefore a significant amount of aerosols will be transported and not fully removed,
400 consistent with findings by (Lee and Wang, 2015; Takeishi and Wang, 2021). This finding is
401 further supported by the observed higher concentration of sulfate to BC ratio, requiring a smaller
402 amount of overall freshly-emitted BC particles, and a longer time in-situ, both of which allow the
403 surviving particles more time and greater opportunity to grow. It is also consistent with the
404 highly humid atmosphere providing plenty of water to facilitate the growth of a shell. As
405 demonstrated in Fig.4(a) the BC core size is less than 220nm, while the remaining 50 to 170nm
406 is found in the shell.

407 Second, during the latter part of the cold season (Fig4c-d)(specifically JF) there is observed
408 to be a large amount of locally dominated aerosol sources (both [Urban] and local [BB]
409 associated with economic activity, solid fuel used for cooking, etc.), which in turn fit well with
410 the observed types (Dumka et al., 2008; Kumar et al., 2015). However, during the earlier part of
411 the cold season, also termed the harvest season (ND), the majority of the sources are influenced
412 by local biomass burning, with the results showing that there is a very absorbing fraction of
413 biomass burning type solely observed during this period of time (Rupakheti et al., 2017). The
414 impact of crops being harvested and some straw being left to dry can be observed in both of
415 these seasons, and is ultimately burned to clear the land, or stored and later burned for heating
416 later in the winter, completely consistent with the observed mixture of [Urban] and [BB] profile
417 match in JF (Engling et al., 2011; Lee and Wang, 2017; Duc et al., 2021). This result is further
418 consistent with works by Rupakheti (2019) who demonstrated that aerosols during the post-
419 monsoon season are mostly associated with the biomass burning. Wan et al (2017) who
420 demonstrated the presence of biomass burning organic aerosol tracers is highest in winter and
421 late autumn compared to other seasons of the year, and Liu and Cohen (2022) who demonstrated
422 that areas in Northeastern India at the same time have a significant underestimate in NO_x
423 emissions associated with biomass burning.

424 Overall, these conditions match well with the extensive use of local brick kilns and rubbish
425 burning occurring in the winter, transport from India and Bangladesh during the monsoon, and
426 burning of straw and other agricultural waste during the harvest season. However, given that the
427 cold period has 2 different phases, further work should be clear about which of the two phases is
428 being indicated when analyzing the impacts of biomass burning in this part of the world.

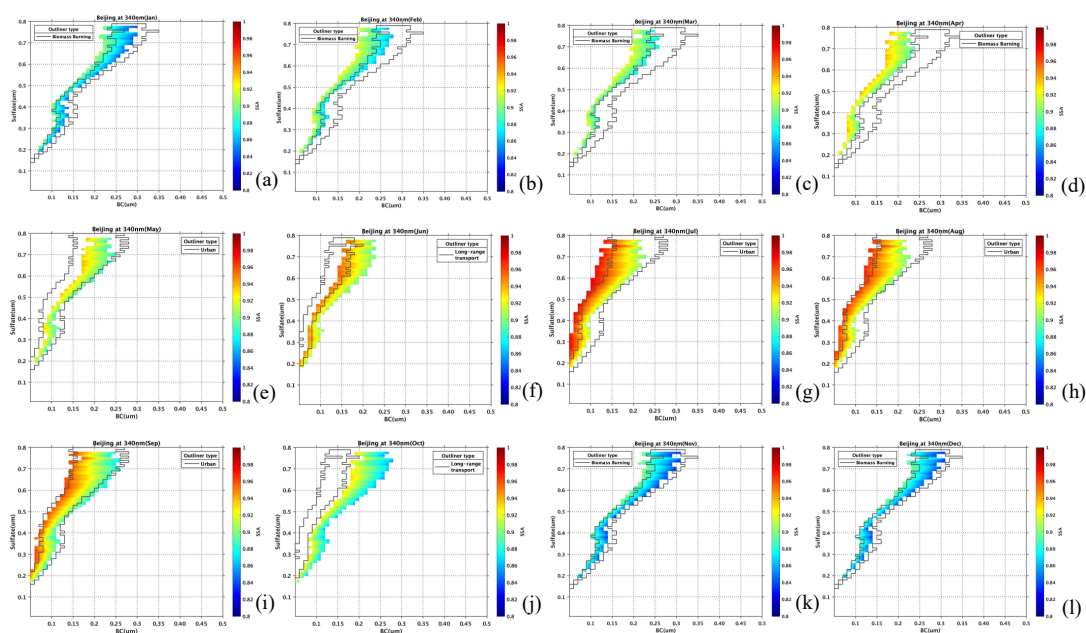


429
 430 **Figure 4.** Constrained distribution of SSA from model result of Lumbini during winter(DJF),
 431 Harvest season and Monsoon with urban, Biomass Burning and Long-range transport profile.

432
 433 Beijing is a highly dense urban area with a very large population, extensive private transport
 434 and without much heavy industry, indicating that an urban profile would generally be expected
 435 to dominate. Figure 5 demonstrates that over 9 months of the year, that there is a very strong
 436 urban signal in the data, when analyzed on a month-by-month basis. However, Beijing is also
 437 located at the foothills of mountainous regions to the West and North, and therefore can be
 438 subject to biomass burning and dust transport due to its unique geography.

439 A deeper investigation of the month-by-month properties show a clear intra-annual pattern
 440 which coherently and smoothly changes on a month-by-month basis, transitioning from one
 441 aerosol type to another, a very different finding from the hundreds of studies grouping Beijing
 442 aerosol properties on a seasonal basis (Liu et al., 2019; Wang et al., 2016; Han et al., 2014; Sun
 443 et al., 2015; Hu et al., 2017; Zhang et al., 2013; Zheng et al., 2005). November and December
 444 demonstrate a strong, narrow, and pure [BB] signal, while January has a strong [BB] signal, but
 445 one which is slightly less narrow. February continues this transition to smaller BC core sizes and
 446 higher SSA values, with the entire pattern from January shifted to the left by 0.03um,
 447 demonstrating a mix of both [BB] and [Urban] signals. March continues this leftward shift and
 448 thickening of the solution space, with nearly all of the results falling in the [Urban] range, while
 449 also comprehensively filling the breadth of the [Urban] signal. Both April and May reveal a pure
 450 [Urban] signal, without [BB] or [LRT] being observed. This is also observed in September, but
 451 in this case, it is transitioning in terms of larger BC cores in the opposite direction from [LRT]
 452 back towards [BB]. In June, the signal shifts further left, with a loss of some [Urban] signal and a
 453 growing signal of [LRT]. In July, the maximum [LRT] contribution is obtained, with the [LRT]
 454 contributing roughly 50% and the [Urban] contributing the remainder. August starts to shift in
 455 the opposite direction, with the BC core size growing, and the fraction of [LRT] decreasing to
 456 40% and the fraction of [Urban] increasing. Finally, in October, the signal is thinner on average

457 and consists of mostly [Urban] signal and a small amount of [BB]. These results are indicative of
 458 the fact that while Beijing is an urban area, and the measurement site is located in the northern
 459 part of the urban core, that the sources of aerosols are highly variable from month-to-month,
 460 including biomass burning from near-by, and long-range-transported sources from beyond the
 461 JingJinJi area. It is hoped that further projects analyzing sources and profiles of absorbing
 462 aerosols in Beijing will look at a higher time frequency and move beyond the season-to-season
 463 approach currently adapted by the community. Some specific examples are that the biomass
 464 burning seems to cut between both the late Autumn and early Winter periods, and that the large
 465 sources of long-range transport seem to mostly exist in early summer, but over a shorter period
 466 than the summer as a whole. The fact that each month except for November and December is
 467 unique, indicates that there are far more complex forces at work.

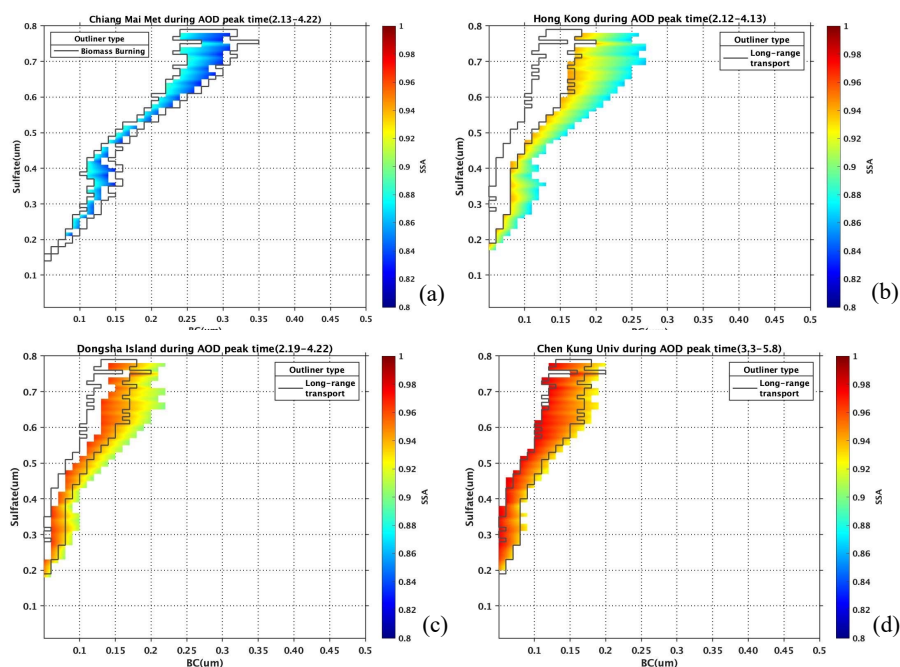


468
 469 **Figure 5.** Constrained distribution of SSA month-by-month, demonstrating Urban, BB, LRT
 470 profiles all during different times of the year.

471 The resulting BC and shell size information during only the high periods of AOD in time (as
 472 displayed in Fig.1) are shown in Fig.6. This focus on when the AOD is highest offers the
 473 perspective of the properties of the BC and shell size when the loadings are most significant.
 474 There is a clear long range transport path observed at both Dongsha Island and Chen Kung
 475 University, and a very small probability of long-range transport identified in Hong Kong, all of
 476 which are consistent with the high biomass burning time periods found throughout Continental
 477 Southeast Asia (Lin et al., 2014; Chan et al., 2003; Lee et al., 2017; Sahu et al., 2014). These
 478 results are found to match very well with the standard [LRT] signal observed in Chiangmai, but
 479 shifted vertically upwards. This result is consistent with the source being biomass burning from
 480 Chiangmai and other surrounding areas (Huang et al., 2013; Fu et al., 2012; Chuang et al., 2015),
 481 which later transports to Dongsha and Chen Kung. While in-route, there is continued in-situ
 482 growth due to SO₂, NO₂, and VOCs from urban areas, and DMS from the South China Sea. The
 483 high time first appears in Hong kong from February 12 through April 13, with only 2% of the
 484 total solution being [LRT], which given the local magnitude of emissions during the dry season

485 in the GBA area (Chen et al., 2020; Duc et al., 2021), may still offer a somewhat significant
 486 impact. The contribution in Dongsha is observed from February 19 to April 22 with a far larger
 487 percentage of of [LRT] at 42%, due to the fact that Dongsha does not have local sources (except
 488 for shipping), but it is still close enough to the GBA that it may contain some not-so-aged
 489 transported aerosols. Finally, the contribution in Chen Kung is observed from March 3 to May 8
 490 and has 62% of [LRT], indicating that long range transport dominates the total loading there,
 491 consistent with the fact that there are very few local sources.

492 Under the assumption that Chiangmai is the source of the biomass burning, the particles will
 493 travel from west to east, first arriving in Hong Kong, next arriving at Dongsha, and finally at
 494 Chen Kung, assuming that the eastern wind in the lower free troposphere is relatively steady
 495 (Wang et al., 2013; Liu et al., 1999). Various one-off experiments and model studies have been
 496 conducted to study the impacts of the annually varying biomass burning events occurring in
 497 Continental Southeast Asia on surrounding areas. While there are many such studies which have
 498 demonstrated the plume in the near-downwind areas including Vietnam, Guangxi and Hainan
 499 (Huang et al., 2020; Ding et al., 2004; Li et al., 2007; Ding et al., 2021; Ding et al., 2013), there
 500 are very few which have been able to successfully transport as far as we have observed here
 501 (Cohen, 2014; Wang et al., 2021). Furthermore, while modeling studies of individual single fire
 502 events transporting in such a manner have been found (Aouizerats et al., 2015; Yen et al., 2013;
 503 Cohen et al., 2017; Wang et al., 2021), there has been no clear observational study, using data
 504 over multiple years (12 at Chen Kung, 10 at Hong Kong, and 6 at Dongsha), in which such a
 505 finding has been made. Furthermore, these findings are not limited in time to a single season or a
 506 single transport event, and provide a comprehensive, fully measurement based analysis.



507
 508 **Figure 6.** Constrained distribution of SSA from model result of sites that located along possible
 509 transport path.

510 4 Applications of Results

511 4.1 In-situ Lifetime of Sulfur Dioxide

512 The computed e-folding time is generally long, consistent with the fact that the air parcels
513 have spent a significant amount of time being transported through the free troposphere, as
514 demonstrated in Table 1. These e-folding times are approximated around the idea of DMS and/or
515 anthropogenic SO₂ decaying into SO⁴⁺ which then condenses onto the shell. The results are not
516 strongly influenced by the quick removal of SO₂ and conversion into H₂SO₄ that occurs in the
517 boundary layer near emissions sources under very high OH, wet and warm conditions found in
518 heavily polluted conditions in this part of the world. Instead, the aging is mainly controlled by
519 gas phase oxidation process happening in cooler and lower pressure air, which is also more likely
520 to be exposed to UV radiation since it is found above the cloud layer. The results therefore
521 should be consistent with relatively higher amounts of OH (closer to urban than background),
522 due in part to the extra amount of UV radiation available above the cloud layer. Additionally, the
523 results should show slower growth due to the lower pressure and cooler conditions. Base on
524 equation (3) the maximum and minimum lifetime of SO₂ in two different chemical background
525 conditions (the background case results are given in the columns of 4 and 5; the urban case
526 results are given in the columns of 6 and 7) are calculated in this manner and listed in Table 1
527 and the possible uncertainty have been evaluated.

528 The results are consistent with the lifetime of SO₂ being longer as compared to the lifetime in
529 the boundary layer where the temperature and recycling of OH are both high. In the free
530 troposphere, although the OH may be high due to stronger UV, the lack of water vapor and
531 VOCs lead to OH regeneration being very slow. Since the lifetime in urban areas is faster, it
532 would make sense that by efficiently reducing the SO₂ emitted from urban areas, the longer
533 timescale the aging of BC and sulfate is reduced (Cohen et al., 2011) for the BC emitted from the
534 biomass burning and subsequently transported downwind over urban areas. Overall, while these
535 lifetimes are long, they are not so long as to be ruled out based on the amount of time it takes to
536 transport from the source region to the measured destination.

537 Testing the values of the e-folding time under background OH conditions yield a maximum
538 lifetime with a value ranging from 21 to 32 days and a minimum ranging from 16 to 20 days.
539 This increase in the amount of time, in particular for the minimum number of days from 10 to 16
540 leads to a set of solutions which are likely not possible. The amount of time required to grow
541 would be more than the amount of time that it would take to be transported. Overall, the breadth
542 of the solution range for lifetime is different between the minimum and maximum cases,
543 consistent with the fact that the decay of atmospheric SO₂ into sulfate is slower than expected,
544 but still reasonable in the case of a higher OH concentration, with the difference from 0 days to 9
545 days. The results require that a significant amount of the total BC is observed above the
546 boundary layer.

547 There are other possible methods and assumptions which could be made to decrease the
548 aging lifetime, which have not been considered herein due to the lack of data. First, higher levels
549 of SO₂ that provided by CAMS, possibly due to increased vertical transport of SO₂ from urban
550 areas along the path of transport, or from heightened DMS emissions or from faster chemical
551 processing of DMS could lead to higher M(env.) in equation 3. Second, this work didn't consider
552 the NO₂+OH reaction to calculate HNO₃, which is optically the same as H₂SO₄ and has the same
553 effect on the result, which will make the in-situ lifetime shorter. Third, this work didn't consider
554 reactions which may occur on the liquid water existing on the coated BC surface (e.g. potentially

555 sulfate aerosol production via aqueous phase oxidation), which would also make the in-situ
 556 lifetime shorter. If all these processes are taken into consideration, it would make the in-situ
 557 lifetime shorter, but not so short that the background OH cases would then be too short to match
 558 with the transport lifetimes. In general, the difference between the max lifetime of background
 559 OH and the min lifetime of urban OH allow the real world observed transport lifetime to be
 560 matched, based on the assumption of whether the oxidation and growth is purely based on the
 561 gas-phase oxidation and equation 1, or whether these other processes are also important.

| Site name | Longitude | Latitude | Max(BG,days) | Min(BG,days) | Max(UR,days) | Min(UR,days) |
|---------------------|-----------|----------|--------------|--------------|--------------|--------------|
| ARM Darwin | 130.891 | -12.425 | 27 | 25 | 17 | 15 |
| ARM Nainital | 79.458 | 29.359 | 23 | 19 | 15 | 12 |
| Anmyon | 126.33 | 36.539 | 25 | 19 | 16 | 13 |
| Bac Giang | 106.225 | 21.291 | 26 | 20 | 17 | 12 |
| Bac Lieu | 105.73 | 9.28 | 22 | 16 | 14 | 10 |
| Baengnyeong | 124.63 | 37.966 | 28 | 22 | 17 | 14 |
| Bandung | 107.61 | -6.888 | 26 | 21 | 16 | 13 |
| Beijing | 116.381 | 39.977 | 30 | 26 | 21 | 17 |
| Beijing-CAMS | 116.317 | 39.933 | 28 | 24 | 18 | 15 |
| Chen-Kung Univ | 120.217 | 23 | 24 | 18 | 15 | 12 |
| Chiang Mai Met Sta | 98.972 | 18.771 | — | — | — | — |
| Chiayi | 120.496 | 23.496 | 26 | 20 | 16 | 13 |
| Darwin | 130.892 | -12.424 | — | — | — | — |
| Dhaka University | 90.398 | 23.728 | 29 | 24 | 19 | 15 |
| Doi Ang Khang | 99.045 | 19.932 | 29 | 23 | 19 | 14 |
| Dongsha Island | 116.729 | 20.699 | 23 | 17 | 14 | 11 |
| EPA-NCU | 121.185 | 24.968 | 26 | 21 | 17 | 13 |
| Fukuoka | 130.475 | 33.524 | 30 | 21 | 19 | 13 |
| Gandhi College | 84.128 | 25.871 | 31 | 23 | 19 | 14 |
| Gangneung WNU | 128.867 | 37.771 | 26 | 20 | 16 | 12 |
| Gosan SNU | 126.162 | 33.292 | 21 | 18 | 13 | 12 |
| Gual Pahari | 77.15 | 28.426 | 31 | 25 | 20 | 15 |
| Gwangju GIST | 126.843 | 35.228 | 26 | 20 | 16 | 12 |
| Hankuk UFS | 127.266 | 37.339 | 29 | 22 | 18 | 14 |
| Hokkaido University | 141.341 | 43.075 | 26 | 21 | 16 | 13 |
| Hong Kong PolyU | 114.18 | 22.303 | 31 | 22 | 19 | 14 |
| Jabiru | 132.893 | -12.661 | 27 | 23 | 17 | 14 |
| Jaipur | 75.806 | 26.906 | 28 | 21 | 18 | 13 |
| Jomsom | 83.714 | 28.778 | 25 | 21 | 16 | 13 |
| KORUS Kyungpook NU | 128.606 | 35.89 | 26 | 21 | 16 | 13 |
| KORUS UNIST Ulsan | 129.19 | 35.582 | 25 | 22 | 15 | 14 |
| Kaashidhoo | 73.466 | 4.965 | 26 | 19 | 16 | 12 |

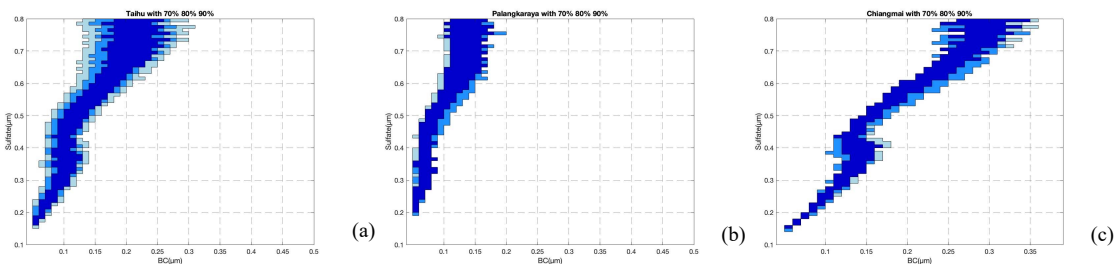
| | | | | | | |
|-------------------|---------|--------|----|----|----|----|
| Kanpur | 80.232 | 26.513 | 31 | 24 | 19 | 15 |
| Kathmandu-Bode | 85.39 | 27.68 | — | — | — | — |
| Kathmandu Univ | 85.538 | 27.601 | 31 | 26 | 19 | 16 |
| Lahore | 74.325 | 31.542 | 31 | 22 | 19 | 14 |
| Luang Namtha | 101.416 | 20.931 | 30 | 23 | 16 | 14 |
| Lumbini | 83.28 | 27.49 | — | — | — | — |
| Mukdahan | 104.676 | 16.607 | 26 | 19 | 16 | 12 |
| NCU Taiwan | 121.192 | 24.967 | 26 | 21 | 17 | 13 |
| NGHIA DO | 105.8 | 21.048 | 27 | 20 | 17 | 13 |
| Nainital | 79.458 | 29.359 | 28 | 22 | 18 | 14 |
| Nong Khai | 102.717 | 17.877 | 29 | 21 | 18 | 13 |
| Noto | 137.137 | 37.334 | 26 | 19 | 16 | 12 |
| Osaka | 135.591 | 34.651 | 24 | 20 | 15 | 12 |
| Palangkaraya | 113.946 | -2.228 | — | — | — | — |
| Pimai | 102.564 | 15.182 | 26 | 20 | 16 | 12 |
| Pokhara | 83.971 | 28.151 | 27 | 26 | 17 | 16 |
| Pune | 73.805 | 18.537 | 31 | 27 | 20 | 17 |
| Pusan NU | 129.083 | 35.235 | 28 | 21 | 17 | 13 |
| SACOL | 104.137 | 35.946 | 32 | 26 | 20 | 16 |
| Seoul SNU | 126.951 | 37.458 | 28 | 21 | 18 | 13 |
| Shirahama | 135.357 | 33.693 | 24 | 18 | 15 | 11 |
| Silpakorn Univ | 100.041 | 13.819 | 29 | 21 | 18 | 13 |
| Singapore | 103.78 | 1.298 | 23 | 18 | 15 | 11 |
| Son La | 103.905 | 21.332 | 30 | 20 | 19 | 13 |
| Songkhla Met Sta | 100.605 | 7.184 | 24 | 17 | 15 | 11 |
| Taihu | 120.215 | 31.421 | — | — | — | — |
| Taipei CWB | 121.5 | 25.03 | 26 | 21 | 17 | 13 |
| Taiping | 114.362 | 10.376 | — | — | — | — |
| USM Penang | 100.302 | 5.358 | 23 | 17 | 14 | 11 |
| Ubon Ratchathani | 104.871 | 15.246 | 25 | 18 | 16 | 11 |
| Ussuriysk | 132.163 | 43.7 | 30 | 23 | 19 | 15 |
| Vientiane | 102.57 | 17.992 | 26 | 20 | 17 | 12 |
| XiangHe | 116.962 | 39.754 | 30 | 23 | 19 | 14 |
| Xinglong | 117.578 | 40.396 | 30 | 22 | 19 | 14 |
| Yonsei University | 126.935 | 37.564 | 24 | 22 | 15 | 14 |
| Yulin | 109.717 | 38.283 | 30 | 29 | 19 | 18 |

563

4.2 Sensitivity of Solutions to Different AERONET Data Assumptions

564 The AERONET measurements contain some data which is of lower or questionable quality
 565 as compared to the bulk of the data. This is frequently due to either not enough absorption to
 566 successfully measure the SSA (i.e., when the $AOD < 0.4$), non-successfully cleared thin clouds, or
 567 other such phenomenon. To account for this uncertainty, this work has previously focused solely
 568 on the middle 80% of the total SSA measurements for each given dataset at each wavelength and
 569 time period studied. By discarding the top and bottom 10%, the reliability of the remaining
 570 measurements is much higher, and therefore the model results are more believable. The fact that
 571 differences on a monthly-basis are already clearly observed is proof that this is a reasonable
 572 approach.

573 However, selecting the central 80% is also arbitrary. So, a further sensitivity study is done to
 574 consider the effects of choosing the central 90% and 70% of data respectively, and quantify the
 575 impact of this cutoff on the computed BC and SO_4 size distributions. The results are given in
 576 Fig.7. A respective use of 70% and 90% of the data lead to a slightly biased change, although not
 577 leading a significant overall difference. In the case of 70% of data, the SSA distribution reduces
 578 by 32%, 27% and 30% respectively in the urban, LRT and BB cases. As observed, there is a
 579 slight bias with the decrease in urban being a further separation from LRT, and the decrease in
 580 BB being a move towards urban. In the case of 90% of data, the SSA distribution increases by
 581 23%, 25.7% and 50% respectively in the urban, LRT and BB cases. As observed, there is a slight
 582 bias in the LRT case, in which case it extends further from the urban and in the BB case, in
 583 which case it also extends further from the urban. However, in all cases, the biases do not
 584 significantly alter the shape, and if anything, make it easier to distinguish the different
 585 underlying factors from each other.



586

587 **Figure.7** SSA distribution of three profiles with different amount of AERONET measurement
 588 data used to constrain the MIE inversion. When the central 70% of the measurements are used,
 589 the results are given in dark blue, when the standard 80% of the measurements are used the
 590 results are given in medium blue, and when the central 90% of the measurements are used the
 591 results are given in light blue. The plot on the left is for Urban, the plot in the center is for LRT,
 592 and the plot on the right is for BB.

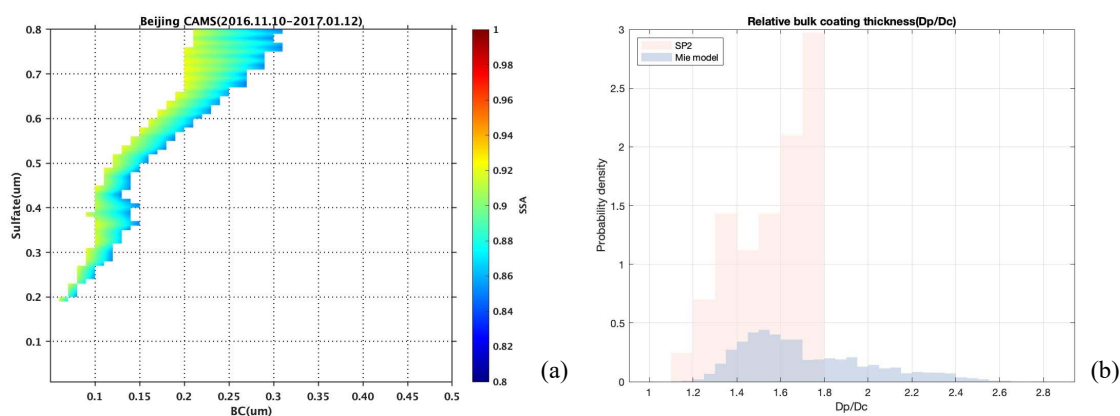
593

4.3 Comparison with Independent Measurements

594 The MIE model inverted core and shell sizes in Beijing overlap at the same time with
 595 measurements taken by SP2 in Beijing from 2016.11.10 to 2017.01.12, as shown in Fig.8a. The
 596 inverted ratio of D_p/D_c from the MIE model approach and as observed from SP2 are shown in
 597 Fig.8b. This comparison assumes that the refractive index of core and shell are the same between
 598 the surface SP2 measurements and the column inverted Mie outputs. In general, the two methods

599 compare well with each other, with nearly all of the SP2 measurements (the 99.5% larger than
 600 1.2) falling within the range of the MIE model inverted results. Next, the bulk of the SP2 data
 601 occurs with a ratio of 1.4-1.6, which also happens to be the mode of the range of outputs of the
 602 MIE model inversion. The only discrepancy is that the MIE model inversion has a range of
 603 values with D_p/D_c larger than 2, which is not observed in the SP2 data.

604 There are a few known possibilities for this discrepancy. First, is that the SP2 may fail to
 605 capture very small particles of BC, which may disaggregate or disintegrate when being hit by the
 606 laser associated with the SP2 detector. Similarly, some of the sulfate shell may be evaporated
 607 due to the heating of the BC, leading to a smaller than actual shell being measured. A third
 608 possible source of disagreement is that the SP2 only measures particles near the ground, while
 609 AERONET measures particles throughout the troposphere, and particles which are aloft as
 610 pointed out already, are more likely to have been in the air longer, and therefore be more
 611 significantly aged, leading to a larger value of D_p/D_c . It is possible that the ageing scale or
 612 transport range observed at the surface urban site may not pick up the fact that there are some
 613 biomass burning aerosols which are mixed into the total column but not necessarily at the
 614 surface, consistent with the fact that 28% of the observed solution space is BB while 72% is
 615 Urban.



616 **Figure.8** Size distribution during overlapping time period between AERONET and SP2
 617 measurement in Beijing(left) plot. Probability density comparison of D_c and D_p/D_c of two
 618 datasets.
 619

620 5 Conclusions

621 Applying a Mie-model with a core-shell approximation over multiple UV bands of the
 622 observed clear sky AERONET SSA has successfully allowed for a new inversion of BC and
 623 shell size and mixing state information to be obtained. These results are observed to group very
 624 well at typical geographical locations with well characterized BC properties. These results help
 625 deepen the understanding of first order chemical aging and particulate growth, and how the
 626 distribution of particle size and absorbing optical characteristics behave under these different
 627 classifications. By narrowly focusing on the size of BC, the size of the refractive shell, and the
 628 mixing state, results are found to be consistent with advanced modeling studies and independent
 629 measurements. The results conform very well over regions that are known to be heavily polluted,
 630 both in terms of urban, biomass burning, long-range transport and mixed sources.

631 Deeper analysis of the temporal and spatial variance, allows for disentanglement of
632 overlapping source types, clearly identifying multiple characteristics as a function of space and
633 time. Some of these characteristics are mixed in time with others, showing that multiple source
634 types are possible to quantify in a probabilistic manner. These results are consistent with the
635 atmospheric column quite reasonably having different sources located near the surface from
636 those observed at the same time in the free troposphere. During specific times, individual sites
637 are observed to rapidly transition from one dominant characteristic state to a different one,
638 indicating significant different sources, atmospheric properties, and driving factors behind the
639 aerosol distribution, even within a single geographic place. Frequently these changes occur at
640 time scales with short temporal duration, although consistently across many different years,
641 indicating new definitions of climate, season, and dynamical driving patterns may be more
642 appropriate to use, rather than standard climatological definitions.

643 The work demonstrates that these types can be successfully divided into three distinct and
644 unique size distributions for [Urban], [BB] and [LRT] conditions. These findings are applied
645 across many different regions in terms of geography, economic development levels, and national
646 boundaries, all of which have their own unique air pollution control rules, environmental goals,
647 and air pollution emissions characterizations. Three excellent examples are observed in Hong
648 Kong, Kathmandu and Beijing. These sites clearly exhibit local sources as expected, but also
649 have periods of time where intense biomass burning, long range transport, and mixtures of these
650 dominate. However, such shifts frequently occur only during specific months, although these
651 patterns are found to hold consistently over many years. In each case, there is an unexpected
652 scientific result: Hong Kong is found to have long-range transport during the Asian Monsoon
653 (usually thought to be clean), associated with LRT transport from Southeast Asia; Nepal is found
654 to have LRT during the monsoon rapidly switching to BB post Asian Monsoon, even when the
655 region experiences the Monsoon rains; and Beijing is exhibited to have all different types
656 slowly shifting from one to another and back, but only observed on a month-by-month basis,
657 vastly different from the typical analyses which group Beijing season-by-season and do not
658 identify these regular occurring and shifting patterns.

659 Based on how these best fit distributions change in time, in specific being shifted from a
660 standard distribution to one with more shell growth, allows for an indirect way to quantify in-situ
661 lifetime. This is clearly observed across many of the sites, allowing for a new observational
662 constraint on the lifetime of aerosols and a quantitative way to constrain the mixing between
663 local and non-local sources. The in-situ age of aerosols at different sites reveals a vast difference
664 in in-situ lifetime, ranging from a week and a half up to a month, based on assumptions of the
665 time of year and pure gas-phase aging and growth. Since these changes are observed throughout
666 the total column, they are reflective of lifetime on a climatological scale, and provide support to
667 many studies which have indicated that absorbing aerosols can transport significant distances,
668 such as across the Pacific Ocean and to the three poles.

669 This work demonstrates that control strategies can be strategically developed for each
670 individual location and adapted during different times of the year. Locations which have a single
671 type would adopt a single strategy, while those with multiple times or time varying types would
672 develop strategies which are multi-perspective and vary from time to time. This approach may
673 allow for significant cost savings and/or more efficient control efforts. Locations with special
674 events could opt for control of different types and amounts during different periods of the year.
675 This flexibility will provide new opportunities to enhance the local atmospheric environment.

676 **Acknowledgments**

677 This work is supported by the National Natural Science Foundation of China (42075147) and the
 678 China University of Mining and Technology Scientific Research Platforms Construction Fund
 679 (102521185). This work thanks the PIs of the AERONET, CAMS for making their data
 680 available.

681

682 **Author contributions**

683 The first draft of the review was prepared by **Xinying Wang**: Conceptualization, Writing -
 684 original draft, Data curation, Writing - review & editing, Investigation, Formal analysis,
 685 Software. **Jason Blake Cohen**: Conceptualization, Data curation, Writing - original draft,
 686 Writing - review & editing, Formal analysis, Funding Acquisition, Supervision. **Shuo Wang**
 687 software and visualization.

688

689 **Data Availability Statement**

690 The AERONET datasets used in this study are available at
 691 https://aeronet.gsfc.nasa.gov/new_web/data_description_AOD_V2.html. The CAMS global
 692 reanalysis product EAC4 is available at
 693 [https://ads.atmosphere.copernicus.eu/cdsapp#!/dataset/cams-global-reanalysis-eac4-](https://ads.atmosphere.copernicus.eu/cdsapp#!/dataset/cams-global-reanalysis-eac4-monthly?tab=overview)
 694 [monthly?tab=overview](https://ads.atmosphere.copernicus.eu/cdsapp#!/dataset/cams-global-reanalysis-eac4-monthly?tab=overview). The SP2 measurements in Beijing are available at
 695 <https://data.ceda.ac.uk/badc/aphh/data/beijing/man-sp2>. All of the data and underlying figures
 696 are available for download at <https://figshare.com/s/a8a98c6dbb7d7b50dabc>.

697

698 **References**

- 699 An, J., Huang, Y., Huang, C., Wang, X., Yan, R., Wang, Q., Wang, H., Jing, S., Zhang, Y., Liu, Y., Chen, Y., Xu,
 700 C., Qiao, L., Zhou, M., Zhu, S., Hu, Q., Lu, J., & Chen, C. (2021). Emission inventory of air pollutants and
 701 chemical speciation for specific anthropogenic sources based on local measurements in the Yangtze River
 702 Delta region, China. In *Atmospheric Chemistry and Physics* (Vol. 21, Issue 3, pp. 2003–2025). Copernicus
 703 GmbH. <https://doi.org/10.5194/acp-21-2003-2021>
- 704 Aouizerats, B., Thouron, O., Tulet, P., Mallet, M., Gomes, L., & Henzing, J. S. (2010). Development of an online
 705 radiative module for the computation of aerosol optical properties in 3-D atmospheric models: validation
 706 during the EUCAARI campaign. In *Geoscientific Model Development* (Vol. 3, Issue 2, pp. 553–564).
 707 Copernicus GmbH. <https://doi.org/10.5194/gmd-3-553-2010>
- 708 Aouizerats, B., van der Werf, G. R., Balasubramanian, R., & Betha, R. (2015). Importance of transboundary
 709 transport of biomass burning emissions to regional air quality in Southeast Asia during a high fire event. In
 710 *Atmospheric Chemistry and Physics* (Vol. 15, Issue 1, pp. 363–373). Copernicus GmbH.
 711 <https://doi.org/10.5194/acp-15-363-2015>
- 712 Bohren, C. F., & Huffman, D. R. (1998). *Absorption and Scattering of Light by Small Particles*. Wiley.
 713 <https://doi.org/10.1002/9783527618156>
- 714 Bollasina, M. A., Ming, Y., Ramaswamy, V., Schwarzkopf, M. D., & Naik, V. (2014). Contribution of local and
 715 remote anthropogenic aerosols to the twentieth century weakening of the South Asian Monsoon. In
 716 *Geophysical Research Letters* (Vol. 41, Issue 2, pp. 680–687). American Geophysical Union (AGU).
 717 <https://doi.org/10.1002/2013gl058183>
- 718 Bond, T. C. (2001). Spectral dependence of visible light absorption by carbonaceous particles emitted from coal
 719 combustion. In *Geophysical Research Letters* (Vol. 28, Issue 21, pp. 4075–4078). American Geophysical
 720 Union (AGU). <https://doi.org/10.1029/2001gl013652>
- 721 Bond, T. C., & Bergstrom, R. W. (2006). *Light Absorption by Carbonaceous Particles: An Investigative Review*. In
 722 *Aerosol Science and Technology* (Vol. 40, Issue 1, pp. 27–67). Informa UK Limited.
 723 <https://doi.org/10.1080/02786820500421521>
- 724 Bond, T. C., Doherty, S. J., Fahey, D. W., Forster, P. M., Berntsen, T., DeAngelo, B. J., Flanner, M. G., Ghan, S.,
 725 Kärcher, B., Koch, D., Kinne, S., Kondo, Y., Quinn, P. K., Sarofim, M. C., Schultz, M. G., Schulz, M.,

- 726 Venkataraman, C., Zhang, H., Zhang, S., ... Zender, C. S. (2013). Bounding the role of black carbon in the
727 climate system: A scientific assessment. In *Journal of Geophysical Research: Atmospheres* (Vol. 118, Issue
728 11, pp. 5380–5552). American Geophysical Union (AGU). <https://doi.org/10.1002/jgrd.50171>
- 729 Chan, C. Y. (2003). Characteristics of biomass burning emission sources, transport, and chemical speciation in
730 enhanced springtime tropospheric ozone profile over Hong Kong. In *Journal of Geophysical Research* (Vol.
731 108, Issue D1). American Geophysical Union (AGU). <https://doi.org/10.1029/2001jd001555>
- 732 Chen, Q.-X., Huang, C.-L., Yuan, Y., Mao, Q.-J., & Tan, H.-P. (2020). Spatiotemporal Distribution of Major
733 Aerosol Types over China Based on MODIS Products between 2008 and 2017. In *Atmosphere* (Vol. 11,
734 Issue 7, p. 703). MDPI AG. <https://doi.org/10.3390/atmos11070703>
- 735 Chen, Y., Morton, D. C., Andela, N., van der Werf, G. R., Giglio, L., & Randerson, J. T. (2017). A pan-tropical
736 cascade of fire driven by El Niño/Southern Oscillation. In *Nature Climate Change* (Vol. 7, Issue 12, pp.
737 906–911). Springer Science and Business Media LLC. <https://doi.org/10.1038/s41558-017-0014-8>
- 738 Chen, Y., Yan, H., Yao, Y., Zeng, C., Gao, P., Zhuang, L., Fan, L., & Ye, D. (2020). Relationships of ozone
739 formation sensitivity with precursors emissions, meteorology and land use types, in Guangdong-Hong
740 Kong-Macao Greater Bay Area, China. In *Journal of Environmental Sciences* (Vol. 94, pp. 1–13). Elsevier
741 BV. <https://doi.org/10.1016/j.jes.2020.04.005>
- 742 Cheng, Y. F., Wiedensohler, A., Eichler, H., Su, H., Gnauk, T., Brüggemann, E., Herrmann, H., Heintzenberg, J.,
743 Slanina, J., & Tuch, T. (2008). Aerosol optical properties and related chemical apportionment at Xinken in
744 Pearl River Delta of China. In *Atmospheric Environment* (Vol. 42, Issue 25, pp. 6351–6372). Elsevier BV.
745 <https://doi.org/10.1016/j.atmosenv.2008.02.034>
- 746 Chi, J., Du, Y., Zhang, Y., Nie, X., Shi, P., & Qu, T. (2019). A new perspective of the 2014/15 failed El Niño as
747 seen from ocean salinity. In *Scientific Reports* (Vol. 9, Issue 1). Springer Science and Business Media
748 LLC. <https://doi.org/10.1038/s41598-019-38743-z>
- 749 Chin, M., Jacob, D. J., Gardner, G. M., Foreman-Fowler, M. S., Spiro, P. A., & Savoie, D. L. (1996). A global three-
750 dimensional model of tropospheric sulfate. In *Journal of Geophysical Research: Atmospheres* (Vol. 101,
751 Issue D13, pp. 18667–18690). American Geophysical Union (AGU). <https://doi.org/10.1029/96jd01221>
- 752 Chuang, C. C., Penner, J. E., Taylor, K. E., Grossman, A. S., & Walton, J. J. (1997). An assessment of the radiative
753 effects of anthropogenic sulfate. In *Journal of Geophysical Research: Atmospheres* (Vol. 102, Issue D3, pp.
754 3761–3778). American Geophysical Union (AGU). <https://doi.org/10.1029/96jd03087>
- 755 Chuang, M.-T., Fu, J. S., Lin, N.-H., Lee, C.-T., Gao, Y., Wang, S.-H., Sheu, G.-R., Hsiao, T.-C., Wang, J.-L., Yen,
756 M.-C., Lin, T.-H., Thongboonchoo, N., & Chen, W.-C. (2015). Simulating the transport and chemical
757 evolution of biomass burning pollutants originating from Southeast Asia during 7-SEAS/2010 Dongsha
758 experiment. In *Atmospheric Environment* (Vol. 112, pp. 294–305). Elsevier BV.
759 <https://doi.org/10.1016/j.atmosenv.2015.04.055>
- 760 Cohen, J. B. (2014). Quantifying the occurrence and magnitude of the Southeast Asian fire climatology. In
761 *Environmental Research Letters* (Vol. 9, Issue 11, p. 114018). IOP Publishing.
762 <https://doi.org/10.1088/1748-9326/9/11/114018>
- 763 Cohen, J. B., & Wang, C. (2014). Estimating global black carbon emissions using a top-down Kalman Filter
764 approach. In *Journal of Geophysical Research: Atmospheres* (Vol. 119, Issue 1, pp. 307–323). American
765 Geophysical Union (AGU). <https://doi.org/10.1002/2013jd019912>
- 766 Cohen, J. B., Lecoq, E., & Hui Loong Ng, D. (2017). Decadal-scale relationship between measurements of
767 aerosols, land-use change, and fire over Southeast Asia. In *Atmospheric Chemistry and Physics* (Vol. 17,
768 Issue 1, pp. 721–743). Copernicus GmbH. <https://doi.org/10.5194/acp-17-721-2017>
- 769 Cohen, J. B., Prinn, R. G., & Wang, C. (2011). The impact of detailed urban-scale processing on the composition,
770 distribution, and radiative forcing of anthropogenic aerosols. In *Geophysical Research Letters* (Vol. 38,
771 Issue 10, p. n/a-n/a). American Geophysical Union (AGU). <https://doi.org/10.1029/2011gl047417>
- 772 Cooke, W. F. (2002). A general circulation model study of the global carbonaceous aerosol distribution. In *Journal*
773 *of Geophysical Research* (Vol. 107, Issue D16). American Geophysical Union (AGU).
774 <https://doi.org/10.1029/2001jd001274>
- 775 Cooke, W. F., Liou, S. C., Cachier, H., & Feichter, J. (1999). Construction of a $1^\circ \times 1^\circ$ fossil fuel emission data set
776 for carbonaceous aerosol and implementation and radiative impact in the ECHAM4 model. In *Journal of*
777 *Geophysical Research: Atmospheres* (Vol. 104, Issue D18, pp. 22137–22162). American Geophysical
778 Union (AGU). <https://doi.org/10.1029/1999jd900187>
- 779 Corrigan, C. E., Ramanathan, V., & Schauer, J. J. (2006). Impact of monsoon transitions on the physical and optical
780 properties of aerosols. In *Journal of Geophysical Research* (Vol. 111, Issue D18). American Geophysical
781 Union (AGU). <https://doi.org/10.1029/2005jd006370>

- 782 Croft, B., Pierce, J. R., & Martin, R. V. (2014). Interpreting aerosol lifetimes using the GEOS-Chem model and
783 constraints from radionuclide measurements. In *Atmospheric Chemistry and Physics* (Vol. 14, Issue 8, pp.
784 4313–4325). Copernicus GmbH. <https://doi.org/10.5194/acp-14-4313-2014>
- 785 Deng, W., Cohen, J. B., Wang, S., & Lin, C. (2021). Improving the understanding between climate variability and
786 observed extremes of global NO₂ over the past 15 years. In *Environmental Research Letters* (Vol. 16, Issue
787 5, p. 054020). IOP Publishing. <https://doi.org/10.1088/1748-9326/abd502>
- 788 Ding, A., Wang, T., & Fu, C. (2013). Transport characteristics and origins of carbon monoxide and ozone in Hong
789 Kong, South China. In *Journal of Geophysical Research: Atmospheres* (Vol. 118, Issue 16, pp. 9475–
790 9488). American Geophysical Union (AGU). <https://doi.org/10.1002/jgrd.50714>
- 791 Ding, A., Wang, T., Zhao, M., Wang, T., & Li, Z. (2004). Simulation of sea-land breezes and a discussion of their
792 implications on the transport of air pollution during a multi-day ozone episode in the Pearl River Delta of
793 China. In *Atmospheric Environment* (Vol. 38, Issue 39, pp. 6737–6750). Elsevier BV.
794 <https://doi.org/10.1016/j.atmosenv.2004.09.017>
- 795 Ding, K., Huang, X., Ding, A., Wang, M., Su, H., Kerminen, V.-M., Petäjä, T., Tan, Z., Wang, Z., Zhou, D., Sun, J.,
796 Liao, H., Wang, H., Carslaw, K., Wood, R., Zuidema, P., Rosenfeld, D., Kulmala, M., Fu, C., ... Andreae,
797 M. O. (2021). Aerosol-boundary-layer-monsoon interactions amplify semi-direct effect of biomass smoke
798 on low cloud formation in Southeast Asia. In *Nature Communications* (Vol. 12, Issue 1). Springer Science
799 and Business Media LLC. <https://doi.org/10.1038/s41467-021-26728-4>
- 800 Dubovik, O., & King, M. D. (2000). A flexible inversion algorithm for retrieval of aerosol optical properties from
801 Sun and sky radiance measurements. In *Journal of Geophysical Research: Atmospheres* (Vol. 105, Issue
802 D16, pp. 20673–20696). American Geophysical Union (AGU). <https://doi.org/10.1029/2000jd900282>
- 803 Dubovik, O., Holben, B., Eck, T. F., Smirnov, A., Kaufman, Y. J., King, M. D., Tanré, D., & Slutsker, I. (2002).
804 Variability of Absorption and Optical Properties of Key Aerosol Types Observed in Worldwide Locations.
805 In *Journal of the Atmospheric Sciences* (Vol. 59, Issue 3, pp. 590–608). American Meteorological Society.
806 [https://doi.org/10.1175/1520-0469\(2002\)059<0590:voaaop>2.0.co;2](https://doi.org/10.1175/1520-0469(2002)059<0590:voaaop>2.0.co;2)
- 807 Duc, H. N., Bang, H. Q., Quan, N. H., & Quang, N. X. (2021). Impact of biomass burnings in Southeast Asia on air
808 quality and pollutant transport during the end of the 2019 dry season. In *Environmental Monitoring and*
809 *Assessment* (Vol. 193, Issue 9). Springer Science and Business Media LLC.
810 <https://doi.org/10.1007/s10661-021-09259-9>
- 811 Dumka, U. C., Kaskaoutis, D. G., Srivastava, M. K., & Devara, P. C. S. (2015). Scattering and absorption properties
812 of near-surface aerosol over Gangetic–Himalayan region: the role of boundary-layer dynamics and long-
813 range transport. In *Atmospheric Chemistry and Physics* (Vol. 15, Issue 3, pp. 1555–1572). Copernicus
814 GmbH. <https://doi.org/10.5194/acp-15-1555-2015>
- 815 Eck, T. F., Holben, B. N., Sinyuk, A., Pinker, R. T., Goloub, P., Chen, H., Chatenet, B., Li, Z., Singh, R. P.,
816 Tripathi, S. N., Reid, J. S., Giles, D. M., Dubovik, O., O'Neill, N. T., Smirnov, A., Wang, P., & Xia, X.
817 (2010). Climatological aspects of the optical properties of fine/coarse mode aerosol mixtures. In *Journal of*
818 *Geophysical Research* (Vol. 115, Issue D19). American Geophysical Union (AGU).
819 <https://doi.org/10.1029/2010jd014002>
- 820 Engling, G., Zhang, Y.-N., Chan, C.-Y., Sang, X.-F., Lin, M., Ho, K.-F., Li, Y.-S., Lin, C.-Y., & Lee, J. J. (2011).
821 Characterization and sources of aerosol particles over the southeastern Tibetan Plateau during the Southeast
822 Asia biomass-burning season. In *Tellus B: Chemical and Physical Meteorology* (Vol. 63, Issue 1, pp. 117–
823 128). Stockholm University Press. <https://doi.org/10.1111/j.1600-0889.2010.00512.x>
- 824 Fang, X., Fan, Q., Li, H., Liao, Z., Xie, J., & Fan, S. (2018). Multi-scale correlations between air quality and
825 meteorology in the Guangdong–Hong Kong–Macau Greater Bay Area of China during 2015–2017. In
826 *Atmospheric Environment* (Vol. 191, pp. 463–477). Elsevier BV.
827 <https://doi.org/10.1016/j.atmosenv.2018.08.018>
- 828 Fu, J. S., Hsu, N. C., Gao, Y., Huang, K., Li, C., Lin, N.-H., & Tsay, S.-C. (2012). Evaluating the influences of
829 biomass burning during 2006 BASE-ASIA: a regional chemical transport modeling. In *Atmospheric*
830 *Chemistry and Physics* (Vol. 12, Issue 9, pp. 3837–3855). Copernicus GmbH. <https://doi.org/10.5194/acp-12-3837-2012>
- 831
- 832 Guha, A., De, B. K., Dhar, P., Banik, T., Chakraborty, M., Roy, R., Choudhury, A., Gogoi, M. M., Babu, S. S., &
833 Moorthy, K. K. (2015). Seasonal Characteristics of Aerosol Black Carbon in Relation to Long Range
834 Transport over Tripura in Northeast India. In *Aerosol and Air Quality Research* (Vol. 15, Issue 3, pp. 786–
835 798). Taiwan Association for Aerosol Research. <https://doi.org/10.4209/aaqr.2014.02.0029>

- 836 Han, L., Cheng, S., Zhuang, G., Ning, H., Wang, H., Wei, W., & Zhao, X. (2015). The changes and long-range
837 transport of PM_{2.5} in Beijing in the past decade. In *Atmospheric Environment* (Vol. 110, pp. 186–195).
838 Elsevier BV. <https://doi.org/10.1016/j.atmosenv.2015.03.013>
- 839 Han, X., Zhang, M., Gao, J., Wang, S., & Chai, F. (2014). Modeling analysis of the seasonal characteristics of haze
840 formation in Beijing. In *Atmospheric Chemistry and Physics* (Vol. 14, Issue 18, pp. 10231–10248).
841 Copernicus GmbH. <https://doi.org/10.5194/acp-14-10231-2014>
- 842 Han, X., Zhang, M., Zhu, L., & Xu, L. (2013). Model analysis of influences of aerosol mixing state upon its optical
843 properties in East Asia. In *Advances in Atmospheric Sciences* (Vol. 30, Issue 4, pp. 1201–1212). Springer
844 Science and Business Media LLC. <https://doi.org/10.1007/s00376-012-2150-4>
- 845 Hansen, G. B. (2009). Calculation of single-scattering albedos: Comparison of Mie results with Hapke
846 approximations. In *Icarus* (Vol. 203, Issue 2, pp. 672–676). Elsevier BV.
847 <https://doi.org/10.1016/j.icarus.2009.05.025>
- 848 Haywood, J. M., & Ramaswamy, V. (1998). Global sensitivity studies of the direct radiative forcing due to
849 anthropogenic sulfate and black carbon aerosols. In *Journal of Geophysical Research: Atmospheres* (Vol.
850 103, Issue D6, pp. 6043–6058). American Geophysical Union (AGU). <https://doi.org/10.1029/97jd03426>
- 851 Haywood, J. M., & Shine, K. P. (1995). The effect of anthropogenic sulfate and soot aerosol on the clear sky
852 planetary radiation budget. In *Geophysical Research Letters* (Vol. 22, Issue 5, pp. 603–606). American
853 Geophysical Union (AGU). <https://doi.org/10.1029/95gl00075>
- 854 Haywood, J. M., & Shine, K. P. (1997). Multi-spectral calculations of the direct radiative forcing of tropospheric
855 sulphate and soot aerosols using a column model. In *Quarterly Journal of the Royal Meteorological Society*
856 (Vol. 123, Issue 543, pp. 1907–1930). Wiley. <https://doi.org/10.1002/qj.49712354307>
- 857 Hu, W., Hu, M., Hu, W.-W., Zheng, J., Chen, C., Wu, Y., & Guo, S. (2017). Seasonal variations in high time-
858 resolved chemical compositions, sources, and evolution of atmospheric submicron aerosols in the megacity
859 Beijing. In *Atmospheric Chemistry and Physics* (Vol. 17, Issue 16, pp. 9979–10000). Copernicus GmbH.
860 <https://doi.org/10.5194/acp-17-9979-2017>
- 861 Huang, C., Meng, L., He, Y., Shang, N., Yu, H., Huang, T., Zhu, A., Yang, H., Zhao, K., & Yao, L. (2022). Spatial
862 variation of particulate black carbon, and its sources in a large eutrophic urban lake in China. In *Science of
863 The Total Environment* (Vol. 803, p. 150057). Elsevier BV.
864 <https://doi.org/10.1016/j.scitotenv.2021.150057>
- 865 Huang, K., Fu, J. S., Hsu, N. C., Gao, Y., Dong, X., Tsay, S.-C., & Lam, Y. F. (2013). Impact assessment of
866 biomass burning on air quality in Southeast and East Asia during BASE-ASIA. In *Atmospheric
867 Environment* (Vol. 78, pp. 291–302). Elsevier BV. <https://doi.org/10.1016/j.atmosenv.2012.03.048>
- 868 Huang, X., Ding, A., Wang, Z., Ding, K., Gao, J., Chai, F., & Fu, C. (2020). Amplified transboundary transport of
869 haze by aerosol–boundary layer interaction in China. In *Nature Geoscience* (Vol. 13, Issue 6, pp. 428–434).
870 Springer Science and Business Media LLC. <https://doi.org/10.1038/s41561-020-0583-4>
- 871 Jacobson, M. Z. (2000). A physically-based treatment of elemental carbon optics: Implications for global direct
872 forcing of aerosols. In *Geophysical Research Letters* (Vol. 27, Issue 2, pp. 217–220). American
873 Geophysical Union (AGU). <https://doi.org/10.1029/1999gl010968>
- 874 Jacobson, M. Z. (2001). Strong radiative heating due to the mixing state of black carbon in atmospheric aerosols. In
875 *Nature* (Vol. 409, Issue 6821, pp. 695–697). Springer Science and Business Media LLC.
876 <https://doi.org/10.1038/35055518>
- 877 Kleidman, R. G., O'Neill, N. T., Remer, L. A., Kaufman, Y. J., Eck, T. F., Tanré, D., Dubovik, O., & Holben, B. N.
878 (2005). Comparison of Moderate Resolution Imaging Spectroradiometer (MODIS) and Aerosol Robotic
879 Network (AERONET) remote-sensing retrievals of aerosol fine mode fraction over ocean. In *Journal of
880 Geophysical Research* (Vol. 110, Issue D22). American Geophysical Union (AGU).
881 <https://doi.org/10.1029/2005jd005760>
- 882 Kompalli, S. K., Babu, S. N. S., Moorthy, K. K., Satheesh, S. K., Gogoi, M. M., Nair, V. S., Jayachandran, V. N.,
883 Liu, D., Flynn, M. J., & Coe, H. (2021). Mixing state of refractory black carbon aerosol in the South Asian
884 outflow over the northern Indian Ocean during winter. In *Atmospheric Chemistry and Physics* (Vol. 21,
885 Issue 11, pp. 9173–9199). Copernicus GmbH. <https://doi.org/10.5194/acp-21-9173-2021>
- 886 Koulouri, E., Saarikoski, S., Theodosi, C., Markaki, Z., Gerasopoulos, E., Kouvarakis, G., Mäkelä, T., Hillamo, R.,
887 & Mihalopoulos, N. (2008). Chemical composition and sources of fine and coarse aerosol particles in the
888 Eastern Mediterranean. In *Atmospheric Environment* (Vol. 42, Issue 26, pp. 6542–6550). Elsevier BV.
889 <https://doi.org/10.1016/j.atmosenv.2008.04.010>
- 890 Kühn, T., Partanen, A.-L., Laakso, A., Lu, Z., Bergman, T., Mikkonen, S., Kokkola, H., Korhonen, H., Räisänen, P.,
891 Streets, D. G., Romakkaniemi, S., & Laaksonen, A. (2014). Climate impacts of changing aerosol emissions

- 892 since 1996. In *Geophysical Research Letters* (Vol. 41, Issue 13, pp. 4711–4718). American Geophysical
893 Union (AGU). <https://doi.org/10.1002/2014gl060349>
- 894 Kumar, M., Tiwari, S., Murari, V., Singh, A. K., & Banerjee, T. (2015). Wintertime characteristics of aerosols at
895 middle Indo-Gangetic Plain: Impacts of regional meteorology and long range transport. In *Atmospheric
896 Environment* (Vol. 104, pp. 162–175). Elsevier BV. <https://doi.org/10.1016/j.atmosenv.2015.01.014>
- 897 Kuwata, M., Kondo, Y., Mochida, M., Takegawa, N., & Kawamura, K. (2007). Dependence of CCN activity of less
898 volatile particles on the amount of coating observed in Tokyo. In *Journal of Geophysical Research* (Vol.
899 112, Issue D11). American Geophysical Union (AGU). <https://doi.org/10.1029/2006jd007758>
- 900 Lau, K. M., & Yang, S. (1997). Climatology and interannual variability of the southeast asian summer monsoon. In
901 *Advances in Atmospheric Sciences* (Vol. 14, Issue 2, pp. 141–162). Springer Science and Business Media
902 LLC. <https://doi.org/10.1007/s00376-997-0016-y>
- 903 Lawrence, M. G., & Lelieveld, J. (2010). Atmospheric pollutant outflow from southern Asia: a review. In
904 *Atmospheric Chemistry and Physics* (Vol. 10, Issue 22, pp. 11017–11096). Copernicus GmbH.
905 <https://doi.org/10.5194/acp-10-11017-2010>
- 906 Lee, H.-H., Bar-Or, R. Z., & Wang, C. (2017). Biomass burning aerosols and the low-visibility events in Southeast
907 Asia. In *Atmospheric Chemistry and Physics* (Vol. 17, Issue 2, pp. 965–980). Copernicus GmbH.
908 <https://doi.org/10.5194/acp-17-965-2017>
- 909 Lee, S.-Y., & Wang, C. (2015). The Response of the South Asian Summer Monsoon to Temporal and Spatial
910 Variations in Absorbing Aerosol Radiative Forcing. In *Journal of Climate* (Vol. 28, Issue 17, pp. 6626–
911 6646). American Meteorological Society. <https://doi.org/10.1175/jcli-d-14-00609.1>
- 912 Li, J., Zhang, G., Guo, L., Xu, W., Li, X., Lee, C. S. L., Ding, A., & Wang, T. (2007). Organochlorine pesticides in
913 the atmosphere of Guangzhou and Hong Kong: Regional sources and long-range atmospheric transport. In
914 *Atmospheric Environment* (Vol. 41, Issue 18, pp. 3889–3903). Elsevier BV.
915 <https://doi.org/10.1016/j.atmosenv.2006.12.052>
- 916 Li, P., Xiao, C., Feng, Z., Li, W., & Zhang, X. (2020). Occurrence frequencies and regional variations in Visible
917 Infrared Imaging Radiometer Suite (VIIRS) global active fires. In *Global Change Biology* (Vol. 26, Issue 5,
918 pp. 2970–2987). Wiley. <https://doi.org/10.1111/gcb.15034>
- 919 Li, X., Cohen, J. B., Qin, K., Geng, H., Wu, L., Wu, X., Yang, C., Zhang, R., and Zhang L. (2022) Mass-Conserving
920 Inversion of NO_x Emissions and Inferred Combustion Technologies in Energy Rich Northern China Based
921 on Multi-Year Daily Remotely Sensed and Continuous Surface Measurements. [*PREPRINT*] *ESSOAr*.
922 <https://doi.org/10.1002/essoar.10512337.1>
- 923 Qin K., Shi J., He Q., Deng W., Wang S., Liu, J., Cohen, J. B. (2022) New Model-Free Daily Inversion of NO_x
924 Emissions using TROPOMI (MCMFE-NO_x): Deducing a See-Saw of Halved Well Regulated Sources and
925 Doubled New Sources. [*PREPRINT*] *ESSOAr*. <https://doi.org/10.1002/essoar.10512010.1>
- 926 Lin, C.-Y., Zhao, C., Liu, X., Lin, N.-H., & Chen, W.-N. (2014). Modelling of long-range transport of Southeast
927 Asia biomass-burning aerosols to Taiwan and their radiative forcings over East Asia. In *Tellus B: Chemical
928 and Physical Meteorology* (Vol. 66, Issue 1, p. 23733). Stockholm University Press.
929 <https://doi.org/10.3402/tellusb.v66.23733>
- 930 Lin, C., Cohen, J. B., Wang, S., Lan, R., & Deng, W. (2020). A new perspective on the spatial, temporal, and
931 vertical distribution of biomass burning: quantifying a significant increase in CO emissions. In
932 *Environmental Research Letters* (Vol. 15, Issue 10, p. 104091). IOP Publishing.
933 <https://doi.org/10.1088/1748-9326/abaa7a>
- 934 Lin, Z. J., Tao, J., Chai, F. H., Fan, S. J., Yue, J. H., Zhu, L. H., Ho, K. F., & Zhang, R. J. (2013). Impact of relative
935 humidity and particles number size distribution on aerosol light extinction in the urban area of Guangzhou.
936 In *Atmospheric Chemistry and Physics* (Vol. 13, Issue 3, pp. 1115–1128). Copernicus GmbH.
937 <https://doi.org/10.5194/acp-13-1115-2013>
- 938 Liu, D., Allan, J. D., Young, D. E., Coe, H., Beddows, D., Fleming, Z. L., Flynn, M. J., Gallagher, M. W., Harrison,
939 R. M., Lee, J., Prevot, A. S. H., Taylor, J. W., Yin, J., Williams, P. I., & Zotter, P. (2014). Size distribution,
940 mixing state and source apportionment of black carbon aerosol in London during wintertime. In
941 *Atmospheric Chemistry and Physics* (Vol. 14, Issue 18, pp. 10061–10084). Copernicus GmbH.
942 <https://doi.org/10.5194/acp-14-10061-2014>
- 943 Liu, H., Chang, W. L., Oltmans, S. J., Chan, L. Y., & Harris, J. M. (1999). On springtime high ozone events in the
944 lower troposphere from Southeast Asian biomass burning. In *Atmospheric Environment* (Vol. 33, Issue 15,
945 pp. 2403–2410). Elsevier BV. [https://doi.org/10.1016/s1352-2310\(98\)00357-4](https://doi.org/10.1016/s1352-2310(98)00357-4)
- 946 Liu, J., & Cohen, J. (2022). Quantifying the Missing Half of Daily NO_x Emissions over South, Southeast and East
947 Asia. Research Square Platform LLC. <https://doi.org/10.21203/rs.3.rs-1613262/v1>

- 948 Liu, J., Chu, B., Chen, T., Liu, C., Wang, L., Bao, X., & He, H. (2018). Secondary Organic Aerosol Formation from
949 Ambient Air at an Urban Site in Beijing: Effects of OH Exposure and Precursor Concentrations. In
950 Environmental Science & Technology (Vol. 52, Issue 12, pp. 6834–6841). American Chemical
951 Society (ACS). <https://doi.org/10.1021/acs.est.7b05701>
- 952 Liu, J., Fan, S., Horowitz, L. W., & Levy, H., II. (2011). Evaluation of factors controlling long-range transport of
953 black carbon to the Arctic. In Journal of Geophysical Research (Vol. 116, Issue D4). American
954 Geophysical Union (AGU). <https://doi.org/10.1029/2010jd015145>
- 955 Liu, J., Wang, P., Zhang, H., Du, Z., Zheng, B., Yu, Q., Zheng, G., Ma, Y., Zheng, M., Cheng, Y., Zhang, Q., & He,
956 K. (2020). Integration of field observation and air quality modeling to characterize Beijing aerosol in
957 different seasons. In Chemosphere (Vol. 242, p. 125195). Elsevier BV.
958 <https://doi.org/10.1016/j.chemosphere.2019.12519>
- 959 Logan, J. A., Megretskaia, I., Nassar, R., Murray, L. T., Zhang, L., Bowman, K. W., Worden, H. M., & Luo, M.
960 (2008). Effects of the 2006 El Niño on tropospheric composition as revealed by data from the Tropospheric
961 Emission Spectrometer (TES). In Geophysical Research Letters (Vol. 35, Issue 3). American Geophysical
962 Union (AGU). <https://doi.org/10.1029/2007gl031698>
- 963 Logan, T., Xi, B., Dong, X., Li, Z., & Cribb, M. (2013). Classification and investigation of Asian aerosol absorptive
964 properties. In Atmospheric Chemistry and Physics (Vol. 13, Issue 4, pp. 2253–2265). Copernicus GmbH.
965 <https://doi.org/10.5194/acp-13-2253-2013>
- 966 Lu, Z., Zhang, Q., & Streets, D. G. (2011). Sulfur dioxide and primary carbonaceous aerosol emissions in China and
967 India, 1996–2010. In Atmospheric Chemistry and Physics (Vol. 11, Issue 18, pp. 9839–9864). Copernicus
968 GmbH. <https://doi.org/10.5194/acp-11-9839-2011>
- 969 Martins, J. V., Artaxo, P., Liousse, C., Reid, J. S., Hobbs, P. V., & Kaufman, Y. J. (1998). Effects of black carbon
970 content, particle size, and mixing on light absorption by aerosols from biomass burning in Brazil. In Journal
971 of Geophysical Research: Atmospheres (Vol. 103, Issue D24, pp. 32041–32050). American Geophysical
972 Union (AGU). <https://doi.org/10.1029/98jd02593>
- 973 May, A. A., Lee, T., McMeeking, G. R., Akagi, S., Sullivan, A. P., Urbanski, S., Yokelson, R. J., & Kreidenweis, S.
974 M. (2015). Observations and analysis of organic aerosol evolution in some prescribed fire smoke plumes.
975 In Atmospheric Chemistry and Physics (Vol. 15, Issue 11, pp. 6323–6335). Copernicus GmbH.
976 <https://doi.org/10.5194/acp-15-6323-2015>
- 977 McMeeking, G. R., Good, N., Petters, M. D., McFiggans, G., & Coe, H. (2011). Influences on the fraction of
978 hydrophobic and hydrophilic black carbon in the atmosphere. In Atmospheric Chemistry and Physics (Vol.
979 11, Issue 10, pp. 5099–5112). Copernicus GmbH. <https://doi.org/10.5194/acp-11-5099-2011>
- 980 Miyakawa, T., Oshima, N., Taketani, F., Komazaki, Y., Yoshino, A., Takami, A., Kondo, Y., & Kanaya, Y. (2017).
981 Alteration of the size distributions and mixing states of black carbon through transport in the boundary
982 layer in east Asia. In Atmospheric Chemistry and Physics (Vol. 17, Issue 9, pp. 5851–5864). Copernicus
983 GmbH. <https://doi.org/10.5194/acp-17-5851-2017>
- 984 MYHRE, G., STORDAL, F., RESTAD, K., & ISAKSEN, I. S. A. (1998). Estimation of the direct radiative forcing
985 due to sulfate and soot aerosols. In Tellus B (Vol. 50, Issue 5, pp. 463–477). Stockholm University Press.
986 <https://doi.org/10.1034/j.1600-0889.1998.t01-4-00005.x>
- 987 Peng, J., Hu, M., Guo, S., Du, Z., Zheng, J., Shang, D., Levy Zamora, M., Zeng, L., Shao, M., Wu, Y.-S., Zheng, J.,
988 Wang, Y., Glen, C. R., Collins, D. R., Molina, M. J., & Zhang, R. (2016). Markedly enhanced absorption
989 and direct radiative forcing of black carbon under polluted urban environments. In Proceedings of the
990 National Academy of Sciences (Vol. 113, Issue 16, pp. 4266–4271). Proceedings of the National Academy
991 of Sciences. <https://doi.org/10.1073/pnas.1602310113>
- 992 Penner, J. E. (1994). Carbonaceous aerosols influencing atmospheric radiation: Black and organic carbon. Office of
993 Scientific and Technical Information (OSTI). <https://doi.org/10.2172/10118242>
- 994 Penner, J. E., Chuang, C. C., & Grant, K. (1998). Climate forcing by carbonaceous and sulfate aerosols. In Climate
995 Dynamics (Vol. 14, Issue 12, pp. 839–851). Springer Science and Business Media LLC.
996 <https://doi.org/10.1007/s003820050259>
- 997 Penner, J. E., Dickinson, R. E., & O'Neill, C. A. (1992). Effects of Aerosol from Biomass Burning on the Global
998 Radiation Budget. In Science (Vol. 256, Issue 5062, pp. 1432–1434). American Association for the
999 Advancement of Science (AAAS). <https://doi.org/10.1126/science.256.5062.1432>
- 1000 Pham, M., Müller, J.-F., Brasseur, G. P., Granier, C., & Mégie, G. (1995). A three-dimensional study of the
1001 tropospheric sulfur cycle. In Journal of Geophysical Research (Vol. 100, Issue D12, p. 26061). American
1002 Geophysical Union (AGU). <https://doi.org/10.1029/95jd02095>

- 1003 Prasad, P., Roja Raman, M., Venkat Ratnam, M., Chen, W.-N., Vijaya Bhaskara Rao, S., Gogoi, M. M., Kompalli,
1004 S. K., Sarat Kumar, K., & Suresh Babu, S. (2018). Characterization of atmospheric Black Carbon over a
1005 semi-urban site of Southeast India: Local sources and long-range transport. In *Atmospheric Research* (Vol.
1006 213, pp. 411–421). Elsevier BV. <https://doi.org/10.1016/j.atmosres.2018.06.024>
- 1007 Quinn, P. K. (2004). Aerosol optical properties measured on board the Ronald H. Brown during ACE-Asia as a
1008 function of aerosol chemical composition and source region. In *Journal of Geophysical Research* (Vol. 109,
1009 Issue D19). American Geophysical Union (AGU). <https://doi.org/10.1029/2003jd004010>
- 1010 Ramanathan, V., Crutzen, P. J., Kiehl, J. T., & Rosenfeld, D. (2001a). Aerosols, Climate, and the Hydrological
1011 Cycle. In *Science* (Vol. 294, Issue 5549, pp. 2119–2124). American Association for the Advancement of
1012 Science (AAAS). <https://doi.org/10.1126/science.1064034>
- 1013 Ramanathan, V., Crutzen, P. J., Lelieveld, J., Mitra, A. P., Althausen, D., Anderson, J., Andreae, M. O., Cantrell,
1014 W., Cass, G. R., Chung, C. E., Clarke, A. D., Coakley, J. A., Collins, W. D., Conant, W. C., Dulac, F.,
1015 Heintzenberg, J., Heymsfield, A. J., Holben, B., Howell, S., ... Valero, F. P. J. (2001b). Indian Ocean
1016 Experiment: An integrated analysis of the climate forcing and effects of the great Indo-Asian haze. In
1017 *Journal of Geophysical Research: Atmospheres* (Vol. 106, Issue D22, pp. 28371–28398). American
1018 Geophysical Union (AGU). <https://doi.org/10.1029/2001jd900133>
- 1019 Restad, K., Isaksen, I. S. A., & Berntsen, T. K. (1998). Global distribution of sulphate in the troposphere. In
1020 *Atmospheric Environment* (Vol. 32, Issue 20, pp. 3593–3609). Elsevier BV. [https://doi.org/10.1016/s1352-2310\(98\)00081-8](https://doi.org/10.1016/s1352-2310(98)00081-8)
- 1021
1022 Rinsland, C. P., Luo, M., Shephard, M. W., Clerbaux, C., Boone, C. D., Bernath, P. F., Chiou, L., & Coheur, P. F.
1023 (2008). Tropospheric emission spectrometer (TES) and atmospheric chemistry experiment (ACE)
1024 measurements of tropospheric chemistry in tropical southeast Asia during a moderate El Niño in 2006. In
1025 *Journal of Quantitative Spectroscopy and Radiative Transfer* (Vol. 109, Issue 10, pp. 1931–1942). Elsevier
1026 BV. <https://doi.org/10.1016/j.jqsrt.2007.12.020>
- 1027 Rupakheti, D., Adhikary, B., Praveen, P. S., Rupakheti, M., Kang, S., Mahata, K. S., Naja, M., Zhang, Q., Panday,
1028 A. K., & Lawrence, M. G. (2017). Pre-monsoon air quality over Lumbini, a world heritage site along the
1029 Himalayan foothills. In *Atmospheric Chemistry and Physics* (Vol. 17, Issue 18, pp. 11041–11063).
1030 Copernicus GmbH. <https://doi.org/10.5194/acp-17-11041-2017>
- 1031 Rupakheti, D., Kang, S., & Rupakheti, M. (2020). Two heavy haze events over Lumbini in southern Nepal:
1032 Enhanced aerosol radiative forcing and heating rates. In *Atmospheric Environment* (Vol. 236, p. 117658).
1033 Elsevier BV. <https://doi.org/10.1016/j.atmosenv.2020.117658>
- 1034 Rupakheti, D., Kang, S., Rupakheti, M., Cong, Z., Panday, A. K., & Holben, B. N. (2019). Identification of
1035 absorbing aerosol types at a site in the northern edge of Indo-Gangetic Plain and a polluted valley in the
1036 foothills of the central Himalayas. In *Atmospheric Research* (Vol. 223, pp. 15–23). Elsevier BV.
1037 <https://doi.org/10.1016/j.atmosres.2019.03.003>
- 1038 Sahu, L. K., & Sheel, V. (2013). Spatio-temporal variation of biomass burning sources over South and Southeast
1039 Asia. In *Journal of Atmospheric Chemistry* (Vol. 71, Issue 1, pp. 1–19). Springer Science and Business
1040 Media LLC. <https://doi.org/10.1007/s10874-013-9275-4>
- 1041 Saiz-Lopez, A., Borge, R., Notario, A., Adame, J. A., Paz, D. de la, Querol, X., Artíñano, B., Gómez-Moreno, F. J.,
1042 & Cuevas, C. A. (2017). Unexpected increase in the oxidation capacity of the urban atmosphere of Madrid,
1043 Spain. In *Scientific Reports* (Vol. 7, Issue 1). Springer Science and Business Media LLC.
1044 <https://doi.org/10.1038/srep45956>
- 1045 Salam, A., Mamoon, H. A., Ullah, Md. B., & Ullah, S. M. (2012). Measurement of the atmospheric aerosol particle
1046 size distribution in a highly polluted mega-city in Southeast Asia (Dhaka-Bangladesh). In *Atmospheric*
1047 *Environment* (Vol. 59, pp. 338–343). Elsevier BV. <https://doi.org/10.1016/j.atmosenv.2012.05.024>
- 1048 Sato, M., Hansen, J., Koch, D., Lacis, A., Ruedy, R., Dubovik, O., Holben, B., Chin, M., & Novakov, T. (2003).
1049 Global atmospheric black carbon inferred from AERONET. In *Proceedings of the National Academy of*
1050 *Sciences* (Vol. 100, Issue 11, pp. 6319–6324). Proceedings of the National Academy of Sciences.
1051 <https://doi.org/10.1073/pnas.0731897100>
- 1052 Saxena, P., & Seigneur, C. (1987). On the oxidation of SO₂ to sulfate in atmospheric aerosols. In *Atmospheric*
1053 *Environment* (1967) (Vol. 21, Issue 4, pp. 807–812). Elsevier BV. [https://doi.org/10.1016/0004-6981\(87\)90077-1](https://doi.org/10.1016/0004-6981(87)90077-1)
- 1054
1055 Schuster, G. L. (2005). Inferring black carbon content and specific absorption from Aerosol Robotic Network
1056 (AERONET) aerosol retrievals. In *Journal of Geophysical Research* (Vol. 110, Issue D10). American
1057 Geophysical Union (AGU). <https://doi.org/10.1029/2004jd004548>

- 1058 Schwarz, J. P., Gao, R. S., Spackman, J. R., Watts, L. A., Thomson, D. S., Fahey, D. W., Ryerson, T. B., Peischl, J.,
1059 Holloway, J. S., Trainer, M., Frost, G. J., Baynard, T., Lack, D. A., de Gouw, J. A., Warneke, C., & Del
1060 Negro, L. A. (2008). Measurement of the mixing state, mass, and optical size of individual black carbon
1061 particles in urban and biomass burning emissions. In *Geophysical Research Letters* (Vol. 35, Issue 13).
1062 American Geophysical Union (AGU). <https://doi.org/10.1029/2008gl033968>
- 1063 Shen, Z., Ming, Y., & Held, I. M. (2020). Using the fast impact of anthropogenic aerosols on regional land
1064 temperature to constrain aerosol forcing. In *Science Advances* (Vol. 6, Issue 32). American Association for
1065 the Advancement of Science (AAAS). <https://doi.org/10.1126/sciadv.abb5297>
- 1066 Smith, A. J. A., & Grainger, R. G. (2014). Simplifying the calculation of light scattering properties for black carbon
1067 fractal aggregates. In *Atmospheric Chemistry and Physics* (Vol. 14, Issue 15, pp. 7825–7836). Copernicus
1068 GmbH. <https://doi.org/10.5194/acp-14-7825-2014>
- 1069 Song, C. H., & Carmichael, G. R. (1999). The aging process of naturally emitted aerosol (sea-salt and mineral
1070 aerosol) during long range transport. In *Atmospheric Environment* (Vol. 33, Issue 14, pp. 2203–2218).
1071 Elsevier BV. [https://doi.org/10.1016/s1352-2310\(98\)00301-x](https://doi.org/10.1016/s1352-2310(98)00301-x)
- 1072 Streets, D. G., Bond, T. C., Carmichael, G. R., Fernandes, S. D., Fu, Q., He, D., Klimont, Z., Nelson, S. M., Tsai, N.
1073 Y., Wang, M. Q., Woo, J.-H., & Yarber, K. F. (2003). An inventory of gaseous and primary aerosol
1074 emissions in Asia in the year 2000. In *Journal of Geophysical Research: Atmospheres* (Vol. 108, Issue
1075 D21). American Geophysical Union (AGU). <https://doi.org/10.1029/2002jd003093>
- 1076 Sun, Y. L., Wang, Z. F., Du, W., Zhang, Q., Wang, Q. Q., Fu, P. Q., Pan, X. L., Li, J., Jayne, J., & Worsnop, D. R.
1077 (2015). Long-term real-time measurements of aerosol particle composition in Beijing, China: seasonal
1078 variations, meteorological effects, and source analysis. In *Atmospheric Chemistry and Physics* (Vol. 15,
1079 Issue 17, pp. 10149–10165). Copernicus GmbH. <https://doi.org/10.5194/acp-15-10149-2015>
- 1080 Takeishi, A., & Wang, C. (2022). Radiative and microphysical responses of clouds to an anomalous increase in fire
1081 particles over the Maritime Continent in 2015. In *Atmospheric Chemistry and Physics* (Vol. 22, Issue 6, pp.
1082 4129–4147). Copernicus GmbH. <https://doi.org/10.5194/acp-22-4129-2022>
- 1083 Tan, H., Liu, L., Fan, S., Li, F., Yin, Y., Cai, M., & Chan, P. W. (2016). Aerosol optical properties and mixing state
1084 of black carbon in the Pearl River Delta, China. In *Atmospheric Environment* (Vol. 131, pp. 196–208).
1085 Elsevier BV. <https://doi.org/10.1016/j.atmosenv.2016.02.003>
- 1086 Tao, J., Zhang, Z., Wu, Y., Zhang, L., Wu, Z., Cheng, P., Li, M., Chen, L., Zhang, R., & Cao, J. (2019). Impact of
1087 particle number and mass size distributions of major chemical components on particle mass scattering
1088 efficiency in urban Guangzhou in southern China. In *Atmospheric Chemistry and Physics* (Vol. 19, Issue
1089 13, pp. 8471–8490). Copernicus GmbH. <https://doi.org/10.5194/acp-19-8471-2019>
- 1090 van der Werf, G. R., Randerson, J. T., Giglio, L., Gobron, N., & Dolman, A. J. (2008). Climate controls on the
1091 variability of fires in the tropics and subtropics. In *Global Biogeochemical Cycles* (Vol. 22, Issue 3, p. n/a-
1092 n/a). American Geophysical Union (AGU). <https://doi.org/10.1029/2007gb003122>
- 1093 Wan, X., Kang, S., Li, Q., Rupakheti, D., Zhang, Q., Guo, J., Chen, P., Tripathee, L., Rupakheti, M., Panday, A. K.,
1094 Wang, W., Kawamura, K., Gao, S., Wu, G., & Cong, Z. (2017). Organic molecular tracers in the
1095 atmospheric aerosols from Lumbini, Nepal, in the northern Indo-Gangetic Plain: influence of biomass
1096 burning. In *Atmospheric Chemistry and Physics* (Vol. 17, Issue 14, pp. 8867–8885). Copernicus GmbH.
1097 <https://doi.org/10.5194/acp-17-8867-2017>
- 1098 Wang, C. (2015). Anthropogenic aerosols and the distribution of past large-scale precipitation change. In
1099 *Geophysical Research Letters* (Vol. 42, Issue 24). American Geophysical Union (AGU).
1100 <https://doi.org/10.1002/2015gl066416>
- 1101 Wang, C., Jeong, G. R., & Mahowald, N. (2009) Particulate absorption of solar radiation: anthropogenic aerosols vs.
1102 dust. In *Atmospheric Chemistry and Physics* (Vol. 9, Issue 12, pp. 3935–3945). Copernicus GmbH.
1103 <https://doi.org/10.5194/acp-9-3935-2009>, 2009
- 1104 Wang, J., Ge, C., Yang, Z., Hyer, E. J., Reid, J. S., Chew, B.-N., Mahmud, M., Zhang, Y., & Zhang, M. (2013).
1105 Mesoscale modeling of smoke transport over the Southeast Asian Maritime Continent: Interplay of sea
1106 breeze, trade wind, typhoon, and topography. In *Atmospheric Research* (Vol. 122, pp. 486–503). Elsevier
1107 BV. <https://doi.org/10.1016/j.atmosres.2012.05.009>
- 1108 Wang, S., Cohen, J. B., Deng, W., Qin, K., & Guo, J. (2021). Using a New Top-Down Constrained Emissions
1109 Inventory to Attribute the Previously Unknown Source of Extreme Aerosol Loadings Observed Annually in
1110 the Monsoon Asia Free Troposphere. In *Earth's Future* (Vol. 9, Issue 7). American Geophysical Union
1111 (AGU). <https://doi.org/10.1029/2021ef002167>
- 1112 Wang, S., Cohen, J. B., Lin, C., & Deng, W. (2020). Constraining the relationships between aerosol height, aerosol
1113 optical depth and total column trace gas measurements using remote sensing and models. In *Atmospheric*

- 1114 Chemistry and Physics (Vol. 20, Issue 23, pp. 15401–15426). Copernicus GmbH.
1115 <https://doi.org/10.5194/acp-20-15401-2020>
- 1116 Wang, X., Heald, C. L., Ridley, D. A., Schwarz, J. P., Spackman, J. R., Perring, A. E., Coe, H., Liu, D., & Clarke,
1117 A. D. (2014). Exploiting simultaneous observational constraints on mass and absorption to estimate the
1118 global direct radiative forcing of black carbon and brown carbon. In *Atmospheric Chemistry and Physics*
1119 (Vol. 14, Issue 20, pp. 10989–11010). Copernicus GmbH. <https://doi.org/10.5194/acp-14-10989-2014>
- 1120 Wang, Y. Q. (2004). The transport pathways and sources of PM₁₀ pollution in Beijing during spring 2001, 2002 and
1121 2003. In *Geophysical Research Letters* (Vol. 31, Issue 14). American Geophysical Union (AGU).
1122 <https://doi.org/10.1029/2004gl019732>
- 1123 Webster, P. J., & Yang, S. (1992). Monsoon and Enso: Selectively Interactive Systems. In *Quarterly Journal of the*
1124 *Royal Meteorological Society* (Vol. 118, Issue 507, pp. 877–926). Wiley.
1125 <https://doi.org/10.1002/qj.49711850705>
- 1126 Wu, J., Fu, C., Xu, Y., Tang, J. P., Wang, W., & Wang, Z. (2008). Simulation of direct effects of black carbon
1127 aerosol on temperature and hydrological cycle in Asia by a Regional Climate Model. In *Meteorology and*
1128 *Atmospheric Physics* (Vol. 100, Issues 1–4, pp. 179–193). Springer Science and Business Media LLC.
1129 <https://doi.org/10.1007/s00703-008-0302-y>
- 1130 Xie, R., & Fang, X. (2019). The unusual 2014–2016 El Niño events: Dynamics, prediction and enlightenments. In
1131 *Science China Earth Sciences* (Vol. 63, Issue 5, pp. 626–633). Springer Science and Business Media LLC.
1132 <https://doi.org/10.1007/s11430-019-9561-2>
- 1133 Xu, W. Q., Sun, Y. L., Chen, C., Du, W., Han, T. T., Wang, Q. Q., Fu, P. Q., Wang, Z. F., Zhao, X. J., Zhou, L. B.,
1134 Ji, D. S., Wang, P. C., & Worsnop, D. R. (2015). Aerosol composition, oxidation properties, and sources in
1135 Beijing: results from the 2014 Asia-Pacific Economic Cooperation summit study. In *Atmospheric*
1136 *Chemistry and Physics* (Vol. 15, Issue 23, pp. 13681–13698). Copernicus GmbH.
1137 <https://doi.org/10.5194/acp-15-13681-2015>
- 1138 Xu, X., Xie, J., Li, Y., Miao, S., & Fan, S. (2022). Measurement report: Vehicle-based multi-lidar observational
1139 study of the effect of meteorological elements on the three-dimensional distribution of particles in the
1140 western Guangdong–Hong Kong–Macao Greater Bay Area. In *Atmospheric Chemistry and Physics* (Vol.
1141 22, Issue 1, pp. 139–153). Copernicus GmbH. <https://doi.org/10.5194/acp-22-139-2022>
- 1142 Yang, S., & Lau, W. K.-M. (n.d.). Interannual variability of the Asian monsoon. In *Springer Praxis Books* (pp. 259–
1143 293). Springer Berlin Heidelberg. https://doi.org/10.1007/3-540-37722-0_6
- 1144 Yang, Y., Liao, H., & Li, J. (2014). Impacts of the East Asian summer monsoon on interannual variations of
1145 summertime surface-layer ozone concentrations over China. In *Atmospheric Chemistry and Physics* (Vol.
1146 14, Issue 13, pp. 6867–6879). Copernicus GmbH. <https://doi.org/10.5194/acp-14-6867-2014>
- 1147 Yao, C., Yang, S., Qian, W., Lin, Z., & Wen, M. (2008). Regional summer precipitation events in Asia and their
1148 changes in the past decades. In *Journal of Geophysical Research* (Vol. 113, Issue D17). American
1149 Geophysical Union (AGU). <https://doi.org/10.1029/2007jd009603>
- 1150 Yen, M.-C., Peng, C.-M., Chen, T.-C., Chen, C.-S., Lin, N.-H., Tzeng, R.-Y., Lee, Y.-A., & Lin, C.-C. (2013).
1151 Climate and weather characteristics in association with the active fires in northern Southeast Asia and
1152 spring air pollution in Taiwan during 2010 7-SEAS/Dongsha Experiment. In *Atmospheric Environment*
1153 (Vol. 78, pp. 35–50). Elsevier BV. <https://doi.org/10.1016/j.atmosenv.2012.11.015>
- 1154 Yu, X., Zhu, B., & Zhang, M. (2009). Seasonal variability of aerosol optical properties over Beijing. In *Atmospheric*
1155 *Environment* (Vol. 43, Issue 26, pp. 4095–4101). Elsevier BV.
1156 <https://doi.org/10.1016/j.atmosenv.2009.03.061>
- 1157 Zamora, M.L., Peng, J., Hu, M., Guo, S., Marrero-Ortiz, W., Shang, D., Zheng, J., Du, Z., Wu, Z., & Zhang, R.
1158 (2019). Wintertime aerosol properties in Beijing. In *Atmospheric Chemistry and Physics* (Vol. 19, Issue 22,
1159 pp. 14329–14338). Copernicus GmbH. <https://doi.org/10.5194/acp-19-14329-14338>
- 1160 Zhang, H., Wang, Z., Guo, P., & Wang, Z. (2009). A modeling study of the effects of direct radiative forcing due to
1161 carbonaceous aerosol on the climate in East Asia. In *Advances in Atmospheric Sciences* (Vol. 26, Issue 1,
1162 pp. 57–66). Springer Science and Business Media LLC. <https://doi.org/10.1007/s00376-009-0057->
- 1163 Zhang, J., Liu, J., Tao, S., & Ban-Weiss, G. A. (2015). Long-range transport of black carbon to the Pacific Ocean
1164 and its dependence on aging timescale. In *Atmospheric Chemistry and Physics* (Vol. 15, Issue 20, pp.
1165 11521–11535). Copernicus GmbH. <https://doi.org/10.5194/acp-15-11521-2015>
- 1166 Zhang, R., Jing, J., Tao, J., Hsu, S.-C., Wang, G., Cao, J., Lee, C. S. L., Zhu, L., Chen, Z., Zhao, Y., & Shen, Z.
1167 (2013). Chemical characterization and source apportionment of
1168 PM_{2.5} in Beijing: seasonal perspective. In *Atmospheric*

- 1169 Chemistry and Physics (Vol. 13, Issue 14, pp. 7053–7074). Copernicus GmbH. <https://doi.org/10.5194/acp->
1170 13-7053-2013
- 1171 Zhang, R., Peng, J., Wang, Y., & Hu, M. (2016). Reply to Boucher et al.: Rate and timescale of black carbon aging
1172 regulate direct radiative forcing. In *Proceedings of the National Academy of Sciences* (Vol. 113, Issue 35).
1173 *Proceedings of the National Academy of Sciences*. <https://doi.org/10.1073/pnas.1610241113>
- 1174 Zhang, Z., Shen, Y., Li, Y., Zhu, B., & Yu, X. (2017). Analysis of extinction properties as a function of relative
1175 humidity using a μ -T-Mie model in Nanjing. In *Atmospheric*
1176 *Chemistry and Physics* (Vol. 17, Issue 6, pp. 4147–4157). Copernicus GmbH. <https://doi.org/10.5194/acp->
1177 17-4147-2017
- 1178 Zheng, M., Salmon, L. G., Schauer, J. J., Zeng, L., Kiang, C. S., Zhang, Y., & Cass, G. R. (2005). Seasonal trends in
1179 PM_{2.5} source contributions in Beijing, China. In *Atmospheric Environment* (Vol. 39, Issue 22, pp. 3967–
1180 3976). Elsevier BV. <https://doi.org/10.1016/j.atmosenv.2005.03.036>
- 1181 Zhu, J., Liao, H., & Li, J. (2012). Increases in aerosol concentrations over eastern China due to the decadal-scale
1182 weakening of the East Asian summer monsoon. In *Geophysical Research Letters* (Vol. 39, Issue 9, p. n/a-
1183 n/a). American Geophysical Union (AGU). <https://doi.org/10.1029/2012gl051428>